scDrugPrio: A framework for the analysis of single-cell transcriptomics to address multiple problems in precision medicine in immune-mediated inflammatory diseases

Samuel Schäfer[1,2], Martin Smelik[1,3], Oleg Sysoev[4], Yelin Zhao[1,3], Desiré Eklund[1], Sandra Lilja[1,5], Mika Gustafsson[6], Holger Heyn[7,8], Antonio Julia[9], István A. Kovács[10,11], Joseph Loscalzo[12], Sara Marsal[9], Huan Zhang[1], Xinxiu Li[1,3], Danuta Gawel[1,5,¤], Hui Wang[11,¤], Mikael Benson[1,3,¤,*]

Affiliations

[1]Centre for Personalised Medicine, Linköping University; Linköping, Sweden.
[2]Department of Gastroenterology and Hepatology, University Hospital, Linköping, Sweden.
[3]Division of ENT, CLINTEC, Karolinska Institute, Stockholm, Sweden.
[4]Division of Statistics and Machine Learning, Department of Computer and Information Science, Linkoping University; Linköping, Sweden.
[5]Mavatar, Inc., Stockholm. Sweden
[6]Division for Bioinformatics, Department of Physics, Chemistry and Biology, Linköping University; Linköping, Sweden.
[7]CNAG-CRG, Centre for Genomic Regulation (CRG), Barcelona Institute of Science and Technology (BIST), 08028 Barcelona, Spain
[8]Universitat Pompeu Fabra (UPF), 08002 Barcelona, Spain
[9]Grup de Recerca de Reumatologia, Institut de Recerca Vall d'Hebron, Barcelona, España
[10]Department of Physics and Astronomy, Northwestern University, Evanston, IL 60208, USA.
[11]Northwestern Institute on Complex Systems, Northwestern University, Evanston, IL 60208, USA.
[12]Division of Cardiovascular Medicine, Channing Division of Network Medicine, Department of Medicine, Brigham and Women's Hospital, Harvard Medical School; Boston, MA, USA.
[13]Jiangsu Key Laboratory of Immunity and Metabolism, Department of Pathogenic Biology and Immunology, Xuzhou Medical University; Jiangsu, China.
[*]Corresponding author: mikael.benson@ki.se
[¤]Joint last authors.

Abstract

Background: Ineffective drug treatment is a major problem for many patients with immune-mediated inflammatory diseases (IMIDs). Important reasons are the lack of systematic solutions for drug prioritisation and repurposing based on characterisation of the complex and heterogeneous cellular and molecular changes in IMIDs.

Methods: Here, we propose a computational framework, scDrugPrio, which constructs network models of inflammatory disease based on single-cell RNA sequencing (scRNA-seq) data. scDrugPrio constructs detailed network models of inflammatory diseases that integrate information on cell type-specific expression changes, altered cellular crosstalk and pharmacological properties for the selection and ranking of thousands of drugs.

Results: scDrugPrio was developed using a mouse model of antigen-induced arthritis and validated by improved precision/recall for approved drugs, as well as extensive *in vitro, in vivo,* and *in silico* studies of drugs that were predicted, but not approved, for the studied diseases. Next, scDrugPrio was applied to multiple sclerosis, Crohn's disease, and psoriatic arthritis, further supporting scDrugPrio through prioritisation of relevant and approved drugs. However, in contrast to the mouse model of arthritis, great interindividual cellular and gene expression differences were found in patients with the same diagnosis. Such differences could explain why some patients did or did not respond to treatment. This explanation was supported by the application of scDrugPrio to scRNA-seq data from eleven individual Crohn's disease patients. The analysis showed great variations in drug predictions between patients, for example, assigning a high rank to anti-TNF treatment in a responder and a low rank in a nonresponder to that treatment.

Conclusion: We propose a computational framework, scDrugPrio, for drug prioritisation based on scRNA-seq of IMID disease. Application to individual patients indicates scDrugPrio's

potential for personalised network-based drug screening on cellulome-, genome-, and drugome-wide scales. For this purpose, we made scDrugPrio into an easy-to-use R package (https://github.com/SDTC-CPMed/scDrugPrio).

Keywords: single-cell RNA sequencing, scRNA-seq, immune-mediated inflammatory disease, drug prioritisation, drug repurposing, drug prediction, digital twin

Introduction

Immune-mediated inflammatory diseases (IMIDs), such as rheumatoid arthritis, Crohn's disease, and psoriatic arthritis, affect millions of people worldwide and can cause chronic pain, disability, and reduced quality of life (1). While new classes of therapies are transforming the management of IMIDs, it is still a general problem that many patients do not achieve remission with mono- (2, 3) or combinatorial therapy (3). This may be due to drug development involving testing drugs on large groups of patients, with the assumption that the drug will work similarly on all patients. Such an approach does not take into account the fact that each individual's genetic makeup and environment are unique, leading to significant variations in drug efficacy and side effects.

Given that IMIDs are known to involve thousands of genes that are variably expressed in different cell types and show temporal and interindividual differences (4, 5), single-cell RNA sequencing (scRNA-seq) provides a promising foundation for the identification of suitable drug treatments (6). Indeed, one pioneering case report described scRNA-guided therapy of one patient with an inflammatory disease (7). The case report described successful outcomes in a patient who did not respond to standard treatment. A limitation was that drug selection was

empirical rather than based on systems-level understanding of the relative importance of disease-associated cell types, pathways, and genes.

Several systematic prediction models for drug selection in cancer exist, in which omics data are leveraged to determine the chemotherapies' "killing potential" of tumour cells (8, 9). However, these models are not immediately translatable to IMIDs as they are 1) trained on large public drug-response data (e.g., GDSC database (10) and PRISM (11)), which are thus far unavailable for IMIDs, and 2) pursuing the eradication of disease-associated cell types. Rather few methodologies are applicable to IMIDs, including 1) identification of all druggable targets (12, 13), 2) targeting enriched pathways (13, 14), 3) network-based proximity calculations (6, 15) or 4) matching of transcriptomic signatures as by Connectivity Map (CMap) (16). A limitation of these approaches is that they are developed using bulk transcriptomics or genetic variants and hence do not possess inherent solutions for rank aggregation for parallel analyses of several cell types, which limits their applicability to scRNA-seq.

Aiming to create a systematic framework for scRNA-seq-based drug prioritisation and repositioning in inflammatory diseases, we hypothesised that the limitations of previous methodologies could be overcome by transposing network-based approaches (6, 15) to a systematic and scalable strategy for network-based virtual drug screening of multicellular disease models (MCDMs). Therefore, we composed a computational framework henceforth referred to as scDrugPrio (**Fig. 1**). Using scRNA-seq-derived differentially expressed genes (DEGs) of either 1) one individual or 2) a group comparison between patients and controls, scDrugPrio starts by identifying cell type-specific drug candidates by considering both proximity in a protein–protein interaction network and biopharmacological criteria. To rank

drug candidates, scDrugPrio calculates two measures, intracellular and extracellular centrality. We used these two measures to capture two important drug properties, namely, 1) proficiency in targeting key disease-associated expression changes in a cell type and 2) the relative importance of the targeted cell type. These measures are then aggregated over all cell types to provide a final drug ranking.

Because of the complexity and heterogeneity of IMIDs, we started by developing scDrugPrio using scRNA-seq data from a mouse model of antigen-induced arthritis. This reduced heterogeneity since the mice are inbred and the disease induced in a standardised way. Moreover, the mouse model allowed extensive *in vitro* and *in vivo* validation studies. To illustrate some potential case-of-use scenarios, we next applied scDrugPrio to cerebrospinal fluid from multiple sclerosis patients and intestinal biopsies from Crohn's disease (CD) patients. Our analyses demonstrated drug selection and ranking capabilities through 1) the prioritisation of known drugs. For antigen-induced arthritis, drug selection was also supported by 2) experimental validation of repurposed drugs and 3) favorable comparison with previous methods. Next, we applied scDrugPrio to paired biopsies from individual CD patients, revealing its ability to capture the significant heterogeneity in individualised therapeutic prioritisations.

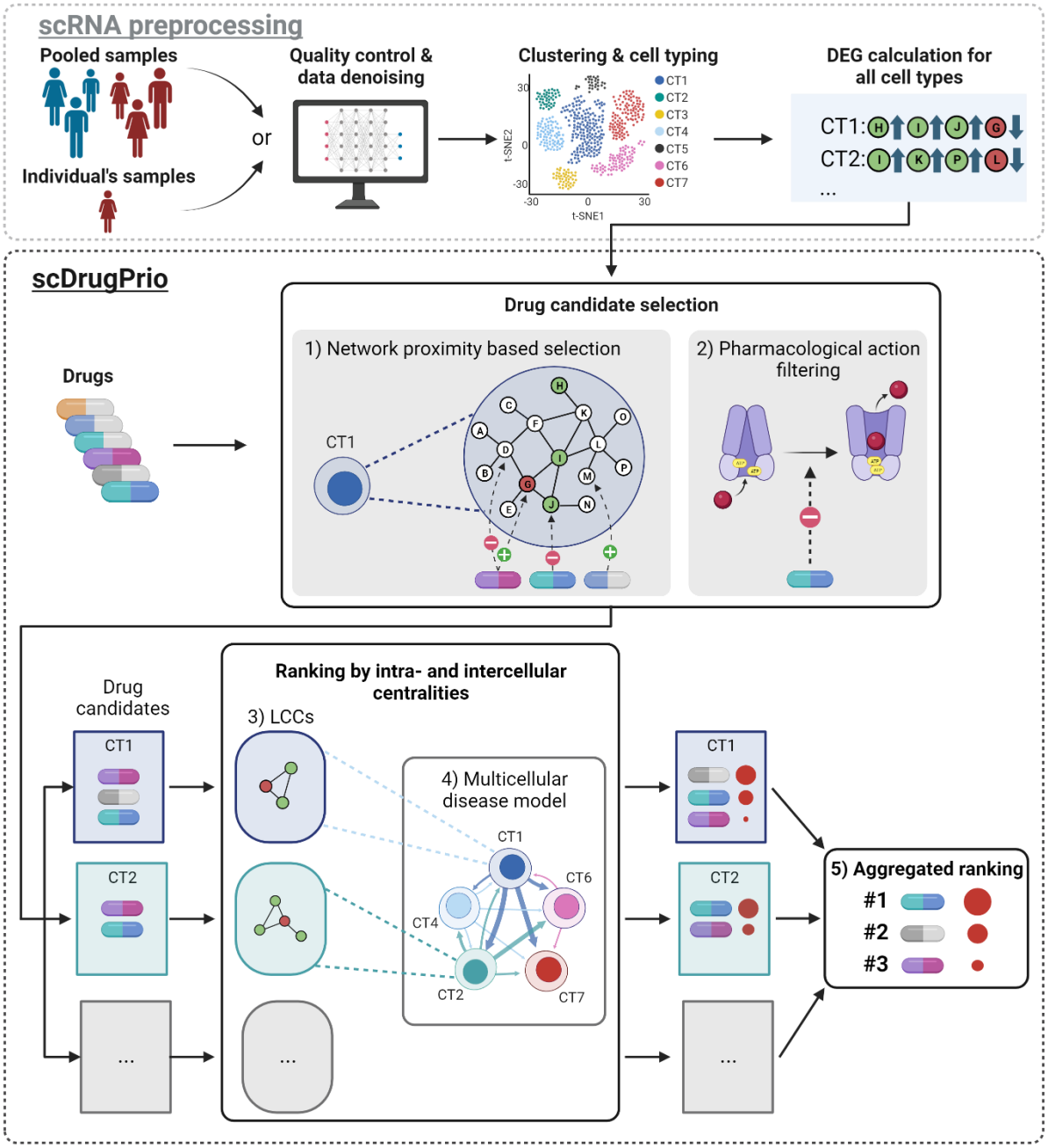

Fig. 1. Overview of the scDrugPrio workflow. Single-cell RNA-sequencing (scRNA-seq) data from either individuals or groups of patients are preprocessed by undergoing quality control, denoising, clustering, cell typing and differentially expressed gene (DEG) calculation. DEGs for each cell type were calculated between healthy and sick samples. Using DEGs alongside information on drugs, scDrugPrio selects drug candidates (for each cell type; CT) whose gene targets are **1)** in network proximity to DEGs and **2)** who counteract disease-

associated expression changes. These cell type-specific drug candidates are next ranked using intracellular and intercellular centrality. **3)** Intracellular centrality is computed based on the centrality of drug targets in the largest connected component (LCC) formed by DEGs and functions as a proxy for drug target importance. **4)** Intercellular centrality measures centrality in disease-associated cellular crosstalk networks called multicellular disease models (MCDMs). **5)** To derive a final ranking that aggregated cell type-specific drug selection and ranking into one list, drug candidates were ranked using a composite score of intra- and intercellular centralities (**Fig. S1**).

Results

The scDrugPrio framework

Aiming to create an analytical framework for scRNA-seq-driven drug prioritisation, we constructed scDrugPrio, which consists of three main modules: 1) drug candidate selection based on cell type-specific DEGs, 2) drug candidate ranking and 3) aggregated ranking of drug candidates from all cell types. For this scDrugPrio requires two components (**Fig. 1**): a) differentially expressed genes (DEGs) between sick and healthy samples for each cell type and b) drug data, including information on gene drug targets and pharmacological effects.

Preprocessing includes the calculation of DEGs based on scRNA expression from one or more healthy and one or more sick samples (**Fig. S1**). Preprocessing starts with quality control, batch correction (if needed) and data denoising of all scRNA-seq data, followed by clustering and cell typing. DEGs are computed per cell type by using sick versus healthy expressions. In the analysis below, we computed DEGs in the two modes. In the first mode, we use data from groups of sick and healthy individuals, while in the second mode, we use scRNA-seq data from paired samples of sick and adjacent healthy tissue for personalised drug prioritisations for one patient of interest.

scDrugPrio starts by computing the mean closest distance between DEGs and gene targets of drugs (henceforth referred to as drug targets) in the protein–protein interaction network (PPIN) for each cell type and each drug candidate. Intuitively, the "closer" the drug targets are to DEGs, the better is the chance for the drug to affect the disease-associated genes (15). Specifically, a relative proximity measure (z_c) capturing the statistical significance of the observed closest distance (d_c) was calculated based on a comparison of d_c to the random expectation.

Furthermore, scDrugPrio assumed that drugs that counteract the fold-change of at least one DEG will have a better chance to reverse disease-associated expression changes in the targeted cell type (following a similar idea as CMap (16)). To determine whether a drug counteracted a DEGs fold change, we considered 1) the direction of the fold change (upregulated or downregulated) and 2) pharmacological action (e.g., agonistic, antagonistic) on the targeted DEG. For each cell type, a list of drug candidates was derived by filtering out drugs with low network proximity ($d_c \geq 1$, $z_c \geq -1.64$ corresponding to one-sided $P < 0.05$) and drugs that did not exert counteracting pharmacological action against at least one targeted DEG.

In the next step, scDrugPrio computed intra- and intercellular centrality measures that were later used to aggregate the prediction and rank drugs. To compute intracellular centralities per cell type, scDrugPrio determines the largest connected component formed by DEGs in the PPIN and next computes a drug's centrality score based on the centrality of the drug targets within this component. Intracellular centrality hence presents an approximation of a drug's target relevance for disease-associated expression changes in a cell type. For intercellular centrality, scDrugPrio constructs a multicellular disease model (MCDM). In short, MCDMs were based on predicted molecular interactions between differentially expressed upstream regulatory genes in any cell type and their downstream genes in any other cell type using NicheNet (17). The resulting MCDM is a network in which cell types were nodes connected by directed, weighted ligand-target interactions. Intercellular centrality refers to the centrality of cell types in the MCDM.

Finally, scDrugPrio aggregates drug predictions through aggregation of cell type-specific drug predictions and intracellular and intercellular centralities into a compound score (**Fig. 1**). The

187 resulting scores were used to rank drugs. Hence, overall drug ranking prioritised drugs that
188 targeted key disease-associated expression changes in the most important cell types.
189
190 *scDrugPrio development and evaluation in antigen-induced arthritis*
191 scRNA-seq data were generated from whole joints of five inbred AIA mice and four naïve mice.
192 After application of quality criteria (**File 1**), data included 16,751 cells with 132,459 mean reads
193 per cell. Data for all mice were denoised jointly using a deep count autoencoder network (DCA)
194 (18), and clusters were cell typed using marker gene expression (**Fig. 2a & S2**). Comparison of
195 cells from AIA and naïve mice identified DEGs in 16 cell types (**Fig. 2, Supplementary**
196 **Results**).
197
198 We retrieved drug target information from DrugBank (19) for 13,339 drugs (**File 1**). From those
199 drugs, we selected all of which had been FDA approved for human use and had at least one
200 target in the human interactome (n = 1,840). According to the indication information in
201 DrugBank, 57 drugs were FDA approved for RA and hence treated as true positives for the
202 calculation of precision and recall.
203
204 Applying scDrugPrio, the final list of candidates included 334 out of 1,840 drugs; 32 drugs
205 were established RA drugs, of which 22 ranked among the top 100 candidates (Fisher exact P
206 $< 10^{-6}$; **Fig. 3, File 1**). To further evaluate the candidates' relevance, we collected clinical trial
207 data from clinicaltrials.gov to capture the medical community's interest in the identified
208 candidates as RA medications. We also performed a literature review of the top 100 drugs to
209 evaluate whether candidates had shown promise when tested in human RA or murine/rat RA
210 models. Through a literature review, evidence for the relevance of 40 additional drugs was

identified, whereas three of the top 100 ranking drugs had not shown effects in previous trials. Hence, 62.0% of the top 100 ranking candidates were either approved or had successful experimental validation in prior literature (**Fig. 3e**), and 95.4% of previously studied top 100 candidates had shown promise.

Describing scDrugPrio results in more detail, network proximity selection (d_c<1, z_c<-1.64) yielded no drug candidates for eight cell types and an average of 67 drug candidates (min = 2, max = 226) for the remaining twelve cell types. Precision among cell type-specific candidates ranged from 0.0% to 12.8%. However, precision of cell types that were central in the MCDM, such as activated, immature, and plasma B cells (12.8%, 11.4%, and 6.3%, respectively), outperformed random selection from the 1,840 included drugs (57/1,840 = 3.1%; Fisher exact $P < 10^{-12}$, $P < 10^{-8}$, $P = 0.4$, respectively). Following network proximity calculations that were performed in the absence of information on a drug's effect on the target, we found tasonermin, a synthetic version of TNF, among the top-ranking candidates for several B-cell subtypes. Since overexpression of TNF has a crucial role in RA pathogenesis (20), this ranking supported the network proximity criterion. However, because tasonermin mimics the effects of TNF, it could worsen the disease. This finding exemplified the importance of pharmacological action selection. Pharmacological action selection resulted in an average of 43 drug candidates per cell type (min = 2, max = 137). Overall precision decreased to a median [range] of 1.56% [0.00 - 20.63], although it increased in activated, immature, and plasma B cells (20.6%, 16.1%, and 9.1%, respectively) as well as in T cells (**Fig. 3c**)

Having identified drug candidates for every cell type individually, intra- and intercellular centrality were calculated. The use of intra- and intercellular centrality measures for composite

ranking was motivated by our findings that 1) intercellular centrality correlated with the significance of GWAS enrichment among cell type-specific DEGs (Pearson's *r* [95% CI] = 0.62 [0.21 – 0.85]; $P < 0.01$), 2) intercellular centrality correlated with the precision among cell type-specific drug candidates (Pearson's *r* [95% CI] = 0.77 [0.46 – 0.91]; $P < 10^{-3}$; **Fig. S2j**), 3) drugs that targeted more than one cell type were more likely to be known RA drugs (**Fig. S2k**) and 4) intracellular centrality could improve the mean rank of known drugs more than expected by chance (**Supplementary Results**).

Using the AIA and human RA data, we benchmarked scDrugPrio against previous methodologies (**Supplementary Results**) and performed extensive additional testing, demonstrating the advantage of scRNA-seq-driven analysis over genetic variations or bulk transcriptomics. Furthermore, we evaluated drug selection criteria and performed robustness analysis (**Supplementary Results).**

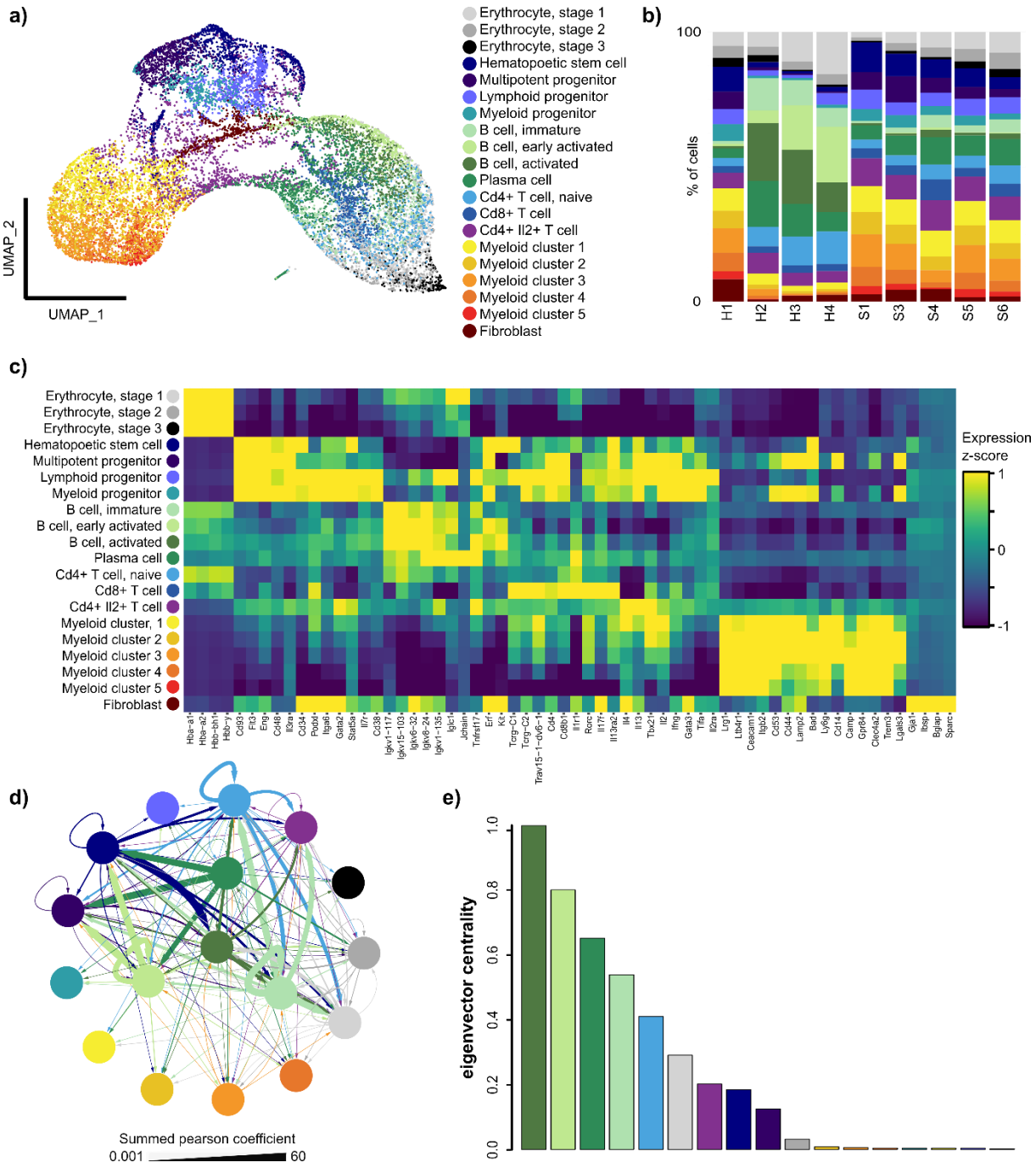

Fig. 2 Construction and analysis of a multicellular disease model (MCDM) based on scRNA-seq analysis of a mouse model of antigen-induced arthritis (AIA). a) tSNE of cells (n = 16,751) pooled from all samples. **b)** Cell type proportions (%) for individual AIA (S1 to S6) and control (H1 to H4) mice. **c)** Heatmap of z-scores of the cluster-based means of normalised, denoised gene expression for cell type markers. **d)** MCDM, in which cell types

were represented by nodes connected by the predicted interactions between upstream regulatory genes in any cell type and their downstream target genes in any other cell type (17). Edge width corresponds to the sum of Pearson coefficients for all interactions between two cell types, with arrows directed from upstream to downstream cell types. Edge color corresponds to the upstream cell type. As indicated by more central positions in the MCDM, the four B-cell clusters were the most central cell types. **e)** Bar plot depicting eigenvector cell type centrality in MCDM. Colours in all plots correspond to cell type colours in a).

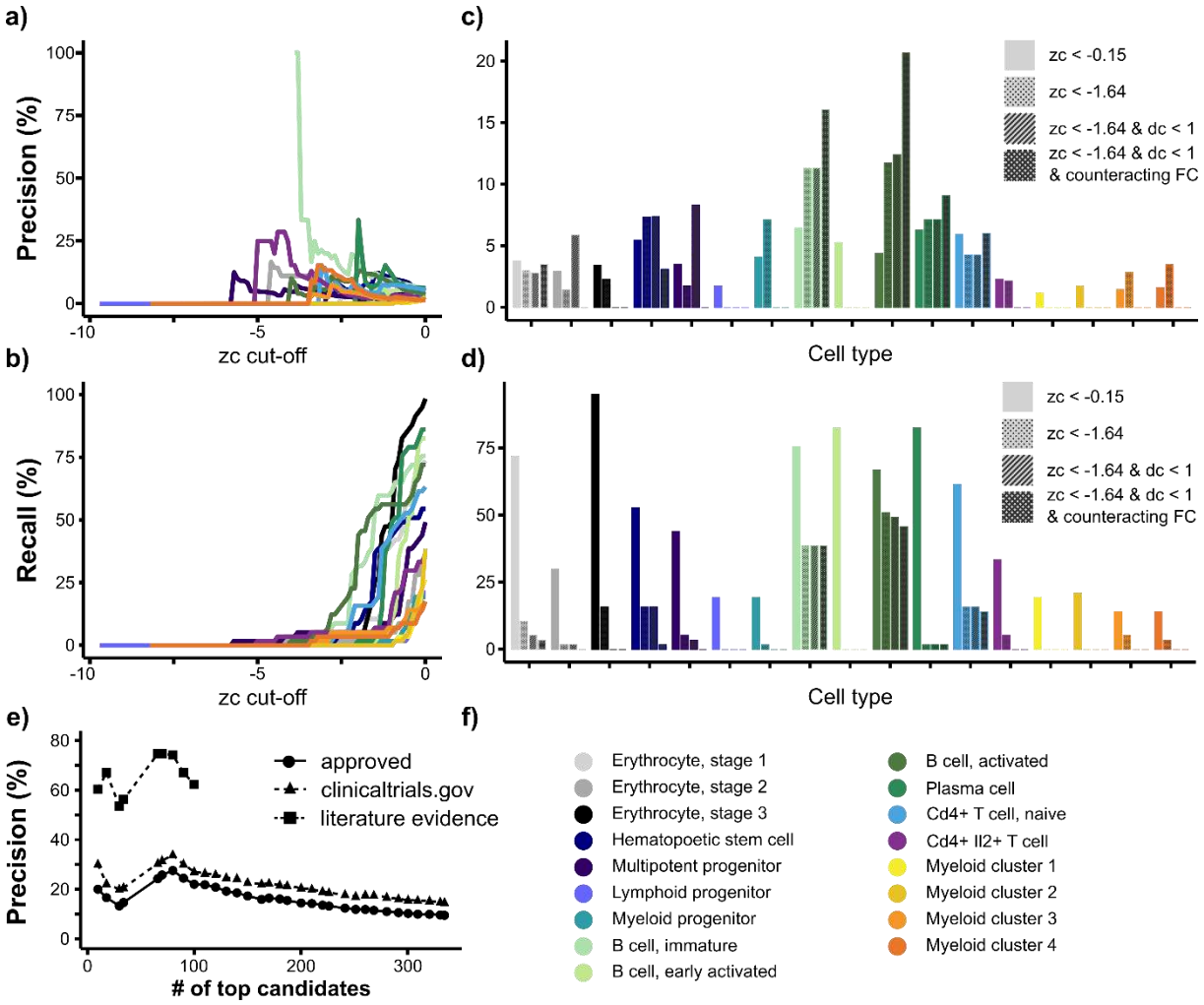

Fig. 3. Precision and recall in relation to drug selection and ranking criteria. a-b) Precision and recall at different z_c cut-offs. In most cell types, precision increased with decreasing z_c. Too stringent z_c cut-offs, by contrast, led to the exclusion of almost all candidates, including approved RA drugs. **c-d)** Precision and recall after stepwise application of drug selection criteria. Bars with no pattern represent a zc cut-off that Guney et al.[10] had previously found to offer good coverage of known drug-disease pairs. The dotted pattern represents precision at $z_c < -1.64$ (corresponding to one-sided $P < 0.05$). The striped pattern represents precision among candidates with $z_c < -1.64$ and $d_c < 1$ (in other words, candidates passing network proximity-based selection). The crosshatch pattern represents candidates passing network proximity and pharmacological action selection. The application of selection criteria substantially increased

the precision among central cell types. **e)** Precision for approved RA drugs and drugs with literature evidence among the ranked list of selected candidates. Drug ranking included rank ties. Literature evidence was gathered for the top 100 ranked candidates and is presented as triangles with a dashed line. The colour legend for **a-d)** is depicted in **f)**.

Experimental validation of scDrugPrio

To further validate scDrugPrio, five high-ranking drugs that were not found to have any prior literature support for their efficacy in RA were chosen alongside the highest-ranking RA drug (auranofin #6) serving as a positive control. We first evaluated the five drugs by *in vitro* studies of B cells. This cell type was selected because of its crucial role in the pathogenesis of RA and its central position in MCDM (21). We used previously described *in vitro* models of B-cell functions (21) measuring murine B-cell survival, activation, proliferation, and antibody production upon *in vitro* stimulation with selected drugs at various concentrations. Auranofin dramatically suppressed B-cell functions, including cell viability, proliferation, and immunoglobulin production (**Fig. 4**). Additionally, two of the five novel drugs (#114 amrinone and #100 adapalene) showed concentration-dependent *in vitro* effects on B-cell viability, proliferation, and immunoglobulin production (**Fig. 4**). Adapalene also greatly inhibited murine B-cell activation (**Fig. 4b**). The other three drugs (#91 irbesartan, #98 isosorbide, and #134 dimethyl furamate) showed little to no effect on murine B-cell functions (**Fig. S3**). Next, we examined the effects of drug candidates on the function of human B cells. Similarly, auranofin, adapalene and amrinone inhibited human B-cell viability, activation, proliferation, and IgG production (**Fig. S4**). Thus, two out of five candidate drugs prioritised by scDrugPrio, namely, adapalene and amrinone, were successfully validated by *in vitro* studies.

298 Valid drug candidates should arguably be transposable and replicable. As drug prediction was
299 performed using data from the AIA model of arthritis, we deployed the collagen-induced
300 arthritis (CIA) model for further *in vivo* study. We selected only amrinone for further study, as
301 adapalene was designed for topical skin use and not for systemic delivery. CIA mice were
302 administered 30 mg/kg amrinone i.g. for 3 weeks. This treatment significantly reduced the paw
303 thickness (**Fig. 4e**) and clinical scores of CIA mice (**Fig. 4f**). Analysis of collagen-specific
304 serum autoantibodies revealed a significant inhibitory effect (**Fig. 4g**). Considering that it even
305 reduced immune cell infiltration (**Fig. 4h**) and bone erosion (**Fig. 4i**), *in vivo* studies confirmed
306 the relevance of amrinone treatment and thereby further supported scDrugPrio.
307

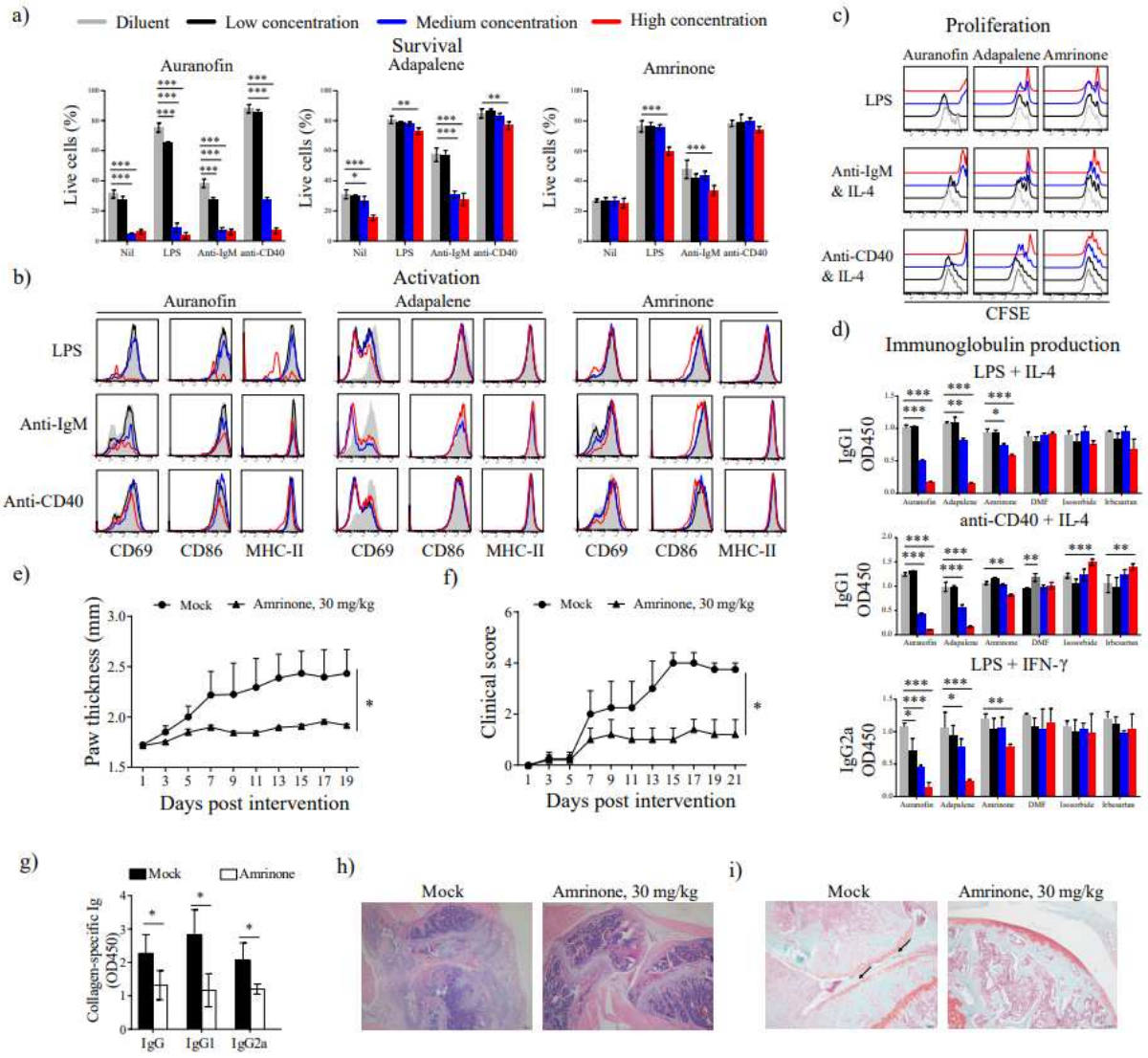

Fig. 4 Experimental validation of amrinone in suppressing murine B-cell function and the pathogenesis of the CIA mouse model. Drug effect of the selected drugs and the positive control on *in vitro* murine **a**) B-cell survival, **b**) activation, **c**) proliferation, and **d**) immunoglobulin production. Colours represent the responses to diluent and different drug concentrations (low, medium, high); for specific concentrations, see **Table S1.** Having successfully validated adapalene and amrinone *in vitro*, we conducted *in vivo* experiments for amrinone. Mice with collagen-induced arthritis (CIA) were treated with diluent (n = 5) or amrinone (30 mg/kg, n = 5) for 3 weeks. The **e)** rear paw thickness, **f)** clinical scores, and **g)**

317 collagen-specific serum autoantibodies were measured. Furthermore, drug efficacy was
318 assessed by analysis of **h)** joint immune cell infiltration using H&E staining and **i)** bone erosion
319 using Safranin-O staining. * $P < 0.05$, ** $P < 0.01$, *** $P < 0.001$. Dimethyl furamate, DMF.
320
321 *Application of scDrugPrio to multiple sclerosis*
322 We next applied scDrugPrio to human IMIDs using scRNA-seq data of cerebrospinal fluid
323 (CSF) from multiple sclerosis (MS) patients and idiopathic intracranial hypertension that served
324 as controls (22). After application of quality cut-offs (**File 2**), the data included 33,848 cells
325 with 47,332 mean reads per cell. Comparing MS samples with controls, DEGs were calculated
326 from batch-corrected, normalised expression scores. scDrugPrio identified on average 59 (min
327 = 1, max = 270) drugs in 19 cell types (**Fig. 5 & S5**). Aggregated ranking of 417 drug candidates
328 (**Fig. S6, File 2**) included ten out of 17 approved MS drugs. Among the top 100 ranking
329 candidates, four approved MS drugs, as well as biosimilars rituximab and obinutuzumab, were
330 identified, which outperformed random expectation (precision 0.9%). A literature search
331 revealed that an additional 22 of the top 100 ranking drugs had shown effects in previous
332 studies, resulting in a precision of 28.3% (**Fig. 5d**). Seventy-one drugs had not yet been
333 validated in previous studies, and one evaluated drug had not shown promise in previous
334 studies. Hence, 96.7% of the studied candidates showed efficacy. Taken together, these data
335 supported the potential of scDrugPrio to predict the response to drugs approved for that disease,
336 as well as for repurposing other drugs.
337
338 The value of above rank aggregation was supported as precision among cell type-specific drug
339 candidates only ranging from 0.0% to 12.5%. The MCDM (**Fig. 5c, File 2**) indicated plasma
340 cells, mononuclear phagocytes, natural killer cells, and activated CD8+ T cells to be of central

importance, which is consistent with the current pathophysiological understanding (22, 23). Notably, the MS MCDM was more complex than the AIA MCDM regarding the number of cell types and interactions.

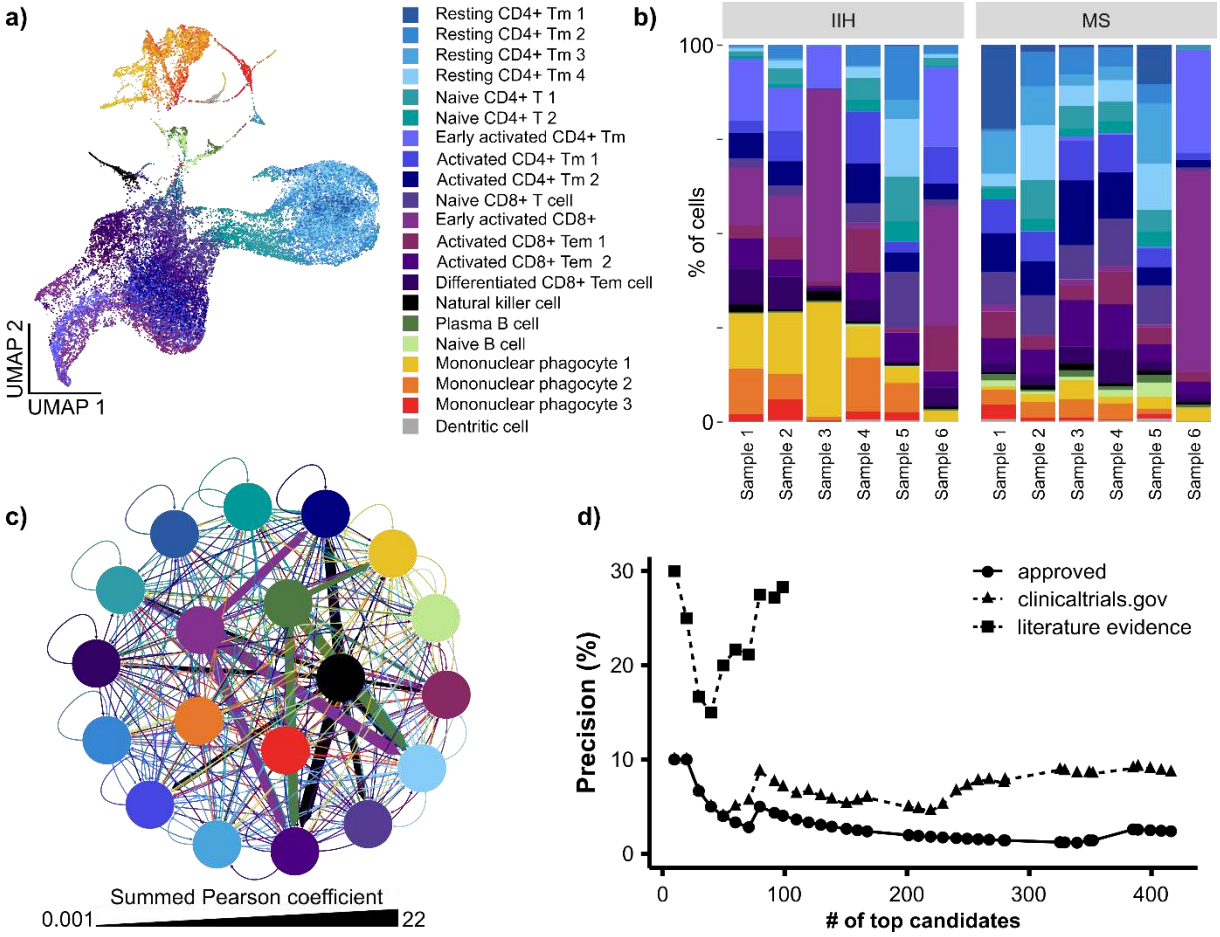

Fig. 5. scDrugPrio applied to scRNA-seq data from cerebrospinal fluid samples of MS patients and controls. a-b) Clustering and cell type proportions (%) for CSF samples of idiopathic intracranial hypertension (IIH) and multiple sclerosis patients (MS). Cell type proportions showed significant interindividual differences among MS patients. **c)** The MCDM for MS was more complex than that of AIA mice. The most central cells included mononuclear phagocyte 3, natural killer cells, mononuclear phagocyte 2, early activated CD8+ T cells and plasma B cells. (in order of eigenvector centrality). **d)** Precision among ranked candidates for

352 approved MS drugs and the top 100 drugs with literature-derived evidence. Abbreviations: Tm,
353 T memory; Tem, T effector memory.
354
355 *Application of scDrugPrio to Crohn's disease*
356 Next, scDrugPrio was applied to patients with Crohn's disease (CD) from whom scRNA-seq
357 data (24) from paired inflamed and uninflamed intestinal tissue biopsies were available. After
358 application of quality criteria (**File 3**), 77,416 cells were included with 3,591 mean unique
359 molecular identifiers (UMIs) per cell. Following preprocessing, analysis was performed on
360 batch-corrected, pooled data from all patients in which DEGs were calculated through
361 comparison of inflamed and uninflamed samples (**Fig. S7 & S8, File 3**). The aggregated ranking
362 included 343 drug candidates, of which five were known CD drugs. These five consisted of
363 sulfasalazine (#91), mesalazine (#169.5), rifaximin (#238) and two anti-TNF drugs
364 (adalimumab and infliximab, tied rank #292.5). Apart from sulfasalazine, literature evidence
365 suggested the effectiveness of 13 additional top-ranking 100 drugs, resulting in a precision of
366 14%.
367
368 *Patient heterogeneity in human disease*
369 An important difference between human data and mouse data was substantial interindividual
370 heterogeneity in human patients. To illuminate such differences, we compared 1) cell type
371 proportions, 2) gene expression profiles and 3) examination of latent features of the non-batch-
372 corrected data. Mice, as expected, showed no differences in cell type proportions (chi-square P
373 = 0.9919; **Fig. 2c**), gene expression (95% CI of misclassification rate 0.504~0.532 in the
374 training data and 0.638-0.655 in the test data), or latent features (**Fig. S2c**). However, both MS
375 and CD patients showed great interindividual heterogeneity in cell type composition (chi-square

376 $P < 10^{-15}$, respectively). Heterogeneity in cell type composition, although decreased, can still
377 be observed in the batch-corrected data (**Fig 5b & S7i**). A patient effect was also observed in
378 the non-batch-corrected gene expression for MS (random forest, 95% CI of misclassification
379 rate 0.075 - 0.084 in training data and 0.124 - 0.132 in testing data) and CD patients (random
380 forest; 95% CI of misclassification rate 0.270 – 0.283 in training data and 0.378 ~ 0.385 in
381 testing data) as well as latent features derived from non-batch-corrected data (**Fig. S5 & S8**).
382 Taken together, such patient effects necessitated batch correction for pooled prediction using
383 the human data sets above.
384
385 *Potential for individualised predictions*
386 Even though batch correction had been applied appropriately, a potential limitation of the above
387 MS and CD analyses was that scDrugPrio was applied to pooled data derived from
388 heterogeneous patients and controls. Patient effects might form the bases for the
389 responder/nonresponder dichotomy, and we therefore evaluated scDrugPrios potential for
390 individualised drug prioritisation. For this, we applied scDrugPrio to individual CD patients,
391 using similar preprocessing as for CD data above with the following exceptions: 1) data were
392 not batch-corrected, and 2) following denoising, cells from inflamed and uninflamed samples
393 of each patient were clustered separately. DEGs were derived through comparison of individual
394 patient inflamed and uninflamed cells in each cluster. DEGs showed that the eleven patients
395 expressed important CD drug targets differently (**Fig. S9a-b**). To investigate whether such
396 molecular differences could affect drug prediction outcomes, scDrugPrio was applied to all
397 patients separately (**Fig. S9-11, File 4**).
398

Strikingly, individualised drug predictions of nine out of eleven patients (such as patient 1: 19.0%; patient 10: 20.5%, **Fig. 6 & S12**) outperformed the precision of pooled patient analysis (14.0%). Among the top 10 candidates, precisions for individualised predictions (20-70%) outperformed precision of pooled patient analysis in seven patients and equalled that of pooled patient analysis in four patients (10%). All predictions outperformed random chance (1.5%). More detailed analysis revealed interindividual differences in cell type proportions and network properties in the MCDM (**Fig. S11**) as well as different drug rankings (**Fig. S13**). Taken together, these findings supported that scDrugPrio presents a valid strategy for personalised drug prioritisation.

To exemplify the potential of scDrugPrio for individual patients, we next compared two patients who previously had been classified as an anti-TNF responder (patient 10) and nonresponder (patient 1) based on a cellular signature score (24). In agreement with the previous classification of anti-TNF response (24), TNF had a more central role in the MCDM of patient 10 (**Fig. S10m, n**). Hence, it was not surprising that aggregated drunk ranking ranked adalimumab (anti-TNF) higher for patient 10 (#15.5) than for patient 1 (#658). As expected, adalimumab was the highest-ranking approved CD drug in patient 10. For patient 1, scDrugPrio prioritised other immunomodulatory drugs over anti-TNF treatment, namely, natalizumab (#19), human intravenous immune globulin (#21), basiliximab (#25), sarilumab (#29), and other approved CD drugs, such as methotrexate (#188) and sulfasalazine (#202).

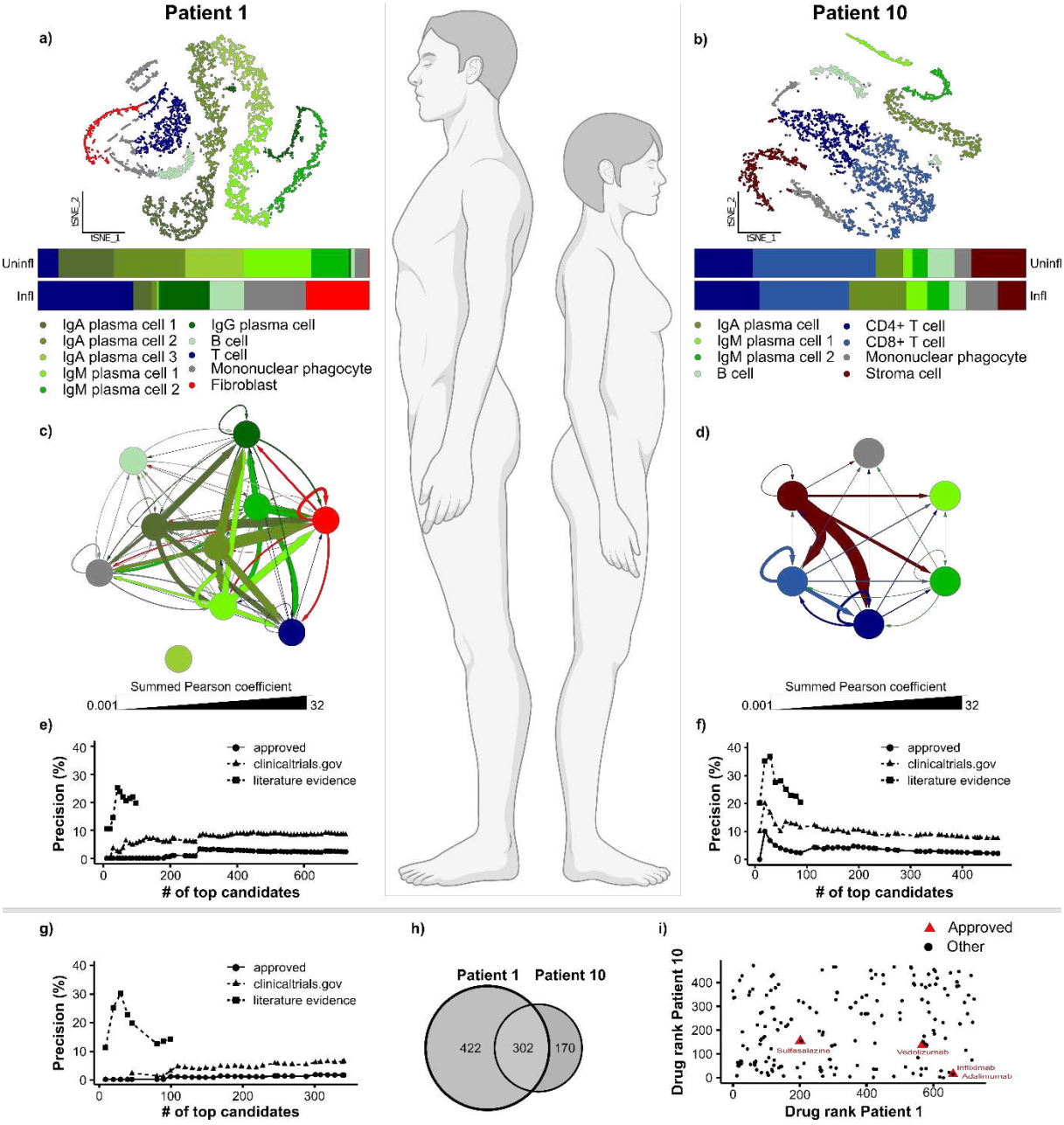

Fig. 6. scDrugPrio for individual drug prediction. a-b) Cell type proportions differed greatly between two CD patients, as shown in the horizontally stacked bar plots representing paired biopsies from inflamed (infl) and uninflamed (uninfl) lesions that were taken from each patient. **c-d)** Patients also show differences in the composition and interconnectivity (representing ligand interactions) of the MCDMs. Patient 1 had a cell type for which no ligand-target interactions could be found with any other cell types in the MCDM. **e-f)** The precision for the

ranked drug candidates for patient 1 was low for approved CD drugs, while literature evidence supported the top-ranking drugs, of which many are anti-inflammatory. In contrast, patient 10 had several approved CD drugs among the top 100 candidates, and a curated literature search confirmed the validity of many more candidates. **g)** Precision for prediction based on pooled patient data was poor. **h)** Venn diagram presenting the overlap of considered drug candidates for patients 1 and 10. **i)** Interindividual differences between patients 1 and 10 were reflected in the prediction outcome, as no correlation existed between the drug rank of drugs that were candidates in both patients.

Application of scDrugPrio to nonresponder/responder data from patients with psoriatic arthritis highlighted the importance of local tissue samples

Since the previous analyses supported scDrugPrio's potential for another case-of-use scenario, namely, to distinguish drug responders from nonresponders. To explore this potential, we collected peripheral mononuclear blood cells (PBMCs) from patients with psoriatic arthritis (PsA) as well as healthy controls. PBMCs were chosen because the analysis of blood samples is clinically more tractable than the analysis of biopsies. Samples were cryopreserved before treatment with either anti-TNF or anti-IL17. Treatment response was later assessed by a rheumatologist according to EULAR response criteria (25) (**File 5**). We next selected 32 patients, of whom eight were classified as responders (R) and eight as nonresponders (NR) to either of the two drugs, as well as eight healthy controls. Cryopreserved PBMCs from these patients were analysed with scRNA-seq. For preprocessing, data were divided into two data sets by treatment regimen, each data set containing the corresponding eight R and NR along with the eight healthy controls. After application of quality cut-offs, the data included 78,610 cells with 5,088 mean reads for anti-TNF analysis and 72,472 cells with 5,343 mean reads for

451 anti-IL17 analysis. Data were batch-corrected and DCA denoised before clusters were
452 identified and cell-typed using marker genes (**Fig. S14 & S15**, **File 5**).
453
454 For each data set, DEGs were calculated through comparison of cells from healthy controls to
455 either R or NR. The precision for approved PsA drugs among the top 100 candidates in the
456 respective aggregated ranking was 0% for anti-IL17 NR, 4% for anti-IL17 R, 1% for anti-TNF
457 NR and 1% for anti-TNF R (**Fig. S14 & S15**). Unexpectedly, anti-TNF treatment received a
458 low rank in anti-TNF R but not in NR (#333 and #88, respectively), while anti-IL-17 was not
459 considered a candidate in either R or NR.
460
461 Further analyses of our PBMC data from all R and NR patients showed that the TNF signaling
462 pathway was significant in only 8% and 8% of clusters, respectively. The corresponding figures
463 for the IL-17 signaling pathway were 17% and 13% in the anti-IL17 R and NR groups,
464 respectively. In those cell types, most pathways were downregulated, including those regulated
465 by *TNF* and *IL17* (**Fig. S16)**. This result contrasted with previous studies of skin and synovium
466 from PsA, which showed increased expression of *TNF* and *IL17*, as well as their pathways (26,
467 27). A similar dichotomy between local inflamed tissues and cells in the blood in autoimmune
468 diseases has been previously described (28). This dichotomy can be explained by the
469 physiological need to localise inflammatory responses to inhibit systemic and possibly fatal
470 responses. The general clinical implication may be that drug predictions should ideally be based
471 on local tissue samples (25).
472

Discussion

The main problem in therapeutics, which serves as the basis for this study, is the large number of IMID patients who do not respond to treatment (2, 3, 29). Previous virtual drug screening methods for inflammatory diseases are based on genetic variance or bulk RNA sequencing (15, 30, 31) and hence do not consider variations in gene expression across different cell types, biopharmacological properties, or individual variations between patients with the same diagnosis. While harnessing the daunting complexity and heterogeneity for personalised treatment may seem impossible by health care standards today, this challenge should be put in the context of the suffering and costs resulting from ineffective drug treatment. Many IMIDs cause life-long morbidity and increased mortality. The yearly cost of treating an individual IMID patient may be hundreds of thousands of dollars for drugs and hospital care (1).

Recent efforts for drug toxicity screening (8, 32) support the feasibility of scRNA-seq to capture relevant cellular information. However, systematic solutions for drug prioritisation for IMIDs based on scRNA-seq remain to be devised. We therefore propose a computational framework, scDrugPrio, that extends on existing bioinformatic tools (6, 15, 17) by providing a framework for data integration, enabling drug ranking based on a multifaceted understanding of cell type-specific disease mechanisms, altered cellular crosstalk and pharmacological effects. We demonstrate that scDrugPrio yields relevant and robust drug prioritisations, outperforms previous methods (14, 33) and holds potential for individualised as well as pooled drug prioritisation and repurposing.

An important advance of scDrugPrio is that it can be applied to scRNA-seq data. The importance lies in the fact that complex diseases each involve differential expression of

497 thousands of genes across multiple cell types (6). A previous case report (7) described one
498 successful example of treating an individual patient with immunological diseases based on
499 scRNA-seq data. However, the drug choices were empirical rather than systematic. Because
500 scRNA-seq allows transcriptome-wide analyses in each of thousands of cells, it is possible to
501 infer disease-associated changes in individual patients preferably by comparisons with
502 noninflamed samples from the same individual or to groups of healthy individuals. Thus,
503 scDrugPrio has the potential to personalise the treatment of individual patients. The importance
504 of this advance is highlighted by our results and previous findings (24, 34) showing great
505 interindividual differences in the molecular and cellular composition of human diseases. For
506 example, we showed that scDrugPrio ranked anti-TNF treatment high in a CD patient who was
507 classified as a responder but not in a nonresponding patient. In the latter patient, other
508 immunomodulatory drugs, such as natalizumab, received high ranks. Natalizumab is mainly
509 used in MS but has, in previous studies, shown positive effects in CD (35), making it a viable
510 recommendation. These examples emphasise that successful drug screening will need to
511 consider variations between patients with the same diagnosis.
512
513 There are several limitations of scRNA-seq-based drug predictions in IMIDs. Many of these
514 depend on the challenges involved in harnessing complex and heterogeneous disease-
515 associated changes with an emerging technology such as scRNA-seq. An analogy to a historical
516 example may illustrate how such limitations may drive scientific progress. In 1970,
517 Needleman–Wunsch (36) and 1981, Smith–Waterman (37) published algorithms for global
518 and local sequence alignment, which were widely used. The limitations of those algorithms
519 were that they were mainly useful for nucleotide but not protein sequence analyses because

of limited protein sequence data and no scoring system that modelled protein evolution. During the next two decades, these problems were resolved by increasingly accurate data and methods (38). Importantly, 42 years after publication of the Smith–Waterman algorithms for proteins, these algorithms can generate very accurate results when combined with scoring systems that were later developed (38). We propose that the limitations of scRNA-seq that we face today will lead to a similar development of increasingly accurate technologies. One obvious limitation of scRNA-seq is that mRNA and protein levels may be poorly correlated, which can limit biological interpretability. From this perspective, the use of DEGs for scDrugPrio's pharmacological predictions is a relative strength, as DEGs have been shown to correlate significantly better with protein levels (39) compared to mRNA levels alone and hence increase the biological relevance of our predictions. Inherent limitations of scDrugPrio also derive from the use of current interactomes, which are not comprehensive in terms of proteins, interactions, and variations across cell types (40) and are prone to investigative biases. While it is impossible to address all these concerns, we explored whether network proximity-based drug selection was influenced by investigative bias through replication of key results in a smaller yet unbiased interactome. We found that precision among candidates was slightly lower, partly due to missing drug targets in the interactome, but that results were comparable. Additionally, scDrugPrio might benefit from systematic parameter optimisation, which is currently not possible due to the limited amount of suitable scRNA-seq data sets.

Predictions were based on complex or partially uncharacterised drug-target effects, which may vary between different locations in the body. The need for better characterised drug effects and the relative importance of drug targets is exemplified by etanercept, which inhibits TNF and its receptors but may activate IgG receptors. The TNF-inhibitory effects are beneficial in PsA,

544 while those on IgG receptors are not clearly defined. However, because all these targets were
545 downregulated in PBMCs from nonresponding PsA patients, etanercept (counteracting IgG
546 downregulation) received a higher rank than in patients responding to anti-TNF treatment.
547 While unexpected, this highlights the need for systematic information about the relative
548 importance of drug targets. Future efforts aiming to address these limitations might find that
549 the predictive capability of scDrugPrio can be further enhanced by integration of binding
550 affinity (e.g., BindingDB) or bioactivity (e.g., ChEMBL), especially if data become more
551 comprehensive.
552
553 The above example of etanercept in PsA highlights an important clinical concern, which to our
554 knowledge has not been recognised in the context of drug prediction methods. While analyses
555 of blood samples are often more tractable in routine clinical practice, disease-associated
556 mechanisms may vary greatly between cells in blood and inflamed tissues. Our scRNA-seq
557 analyses of PBMCs from PsA patients who did or did not respond to treatment with either anti-
558 TNF or anti-IL-17 showed that TNF and IL-17 signaling was found only in a small portion of
559 the PBMC cell types and, in fact, was downregulated in both responders and nonresponders. In
560 contrast, previous studies (26, 27) of synovium from PsA patients have shown consistent
561 upregulation of both signaling pathways. Additionally, one previous study also showed
562 differences between synovium and skin from the same patients (26). Thus, scDrugPrio should
563 ideally be applied to local, inflamed tissue samples of the relevant tissue.
564
565 Despite these limitations, the translational relevance of scDrugPrio was supported by analyses
566 of precision/recall for drugs that were approved for the studied diseases, as well as by *in vitro*
567 and *in vivo* experiments. Those experiments implied two drugs, namely, adapalene (used for

568 acne vulgaris) and amrinone (used for congestive heart failure), that had not been previously
569 described as candidates for RA treatment. However, both have anti-inflammatory effects and
570 could, therefore, be effective (41, 42). This potential was supported by *in vivo* experiments in
571 which CIA mice were treated with amrinone (adapalene is a topical skin drug and hence is not
572 suitable for systemic treatment in this experimental system). This example also suggests a
573 potentially important pharmacological application of scDrugPrio, namely, virtual drug
574 repurposing by systematic screening of thousands of drugs across several inflammatory
575 diseases, as well as in patients who do not respond to standard treatment.
576
577 Here, we show that scDrugPrio has the potential for individualised drug predictions. We have
578 made data and tools freely available for this purpose. However, further parameter optimisation
579 and controlled, prospective clinical studies are needed for clinical translation. If successful, this
580 approach could lead to a radical change in health care, which today is largely based on treating
581 groups of patients with the same diagnosis with a limited number of drugs based on a limited
582 understanding of the underlying molecular complexity and heterogeneity with limited
583 population-based efficacy (43).
584

585 ## Acknowledgement

586 This work was supported by This work is supported by Doctis project, which has received
587 funding from the European Union's Horizon 2020 Research and Innovation Programme under
588 Grant Agreement N° 848028; Swedish Cancer Society CAN 2017/411; Cocozza Foundation;
589 National Natural Science Foundation of China 82171791, US National Institutes of Health
590 grants HL155107 and HL155096; American Heart Association grant 957729; European
591 Union's Horizon 2021 Research and Innovation Programme grant 101057619 and Mag-

592 Tarmfonden (grant 1-23). The computations were partially enabled by resources provided by
593 the Swedish National Infrastructure for Computing (SNIC) at Linköping University partially
594 funded by the Swedish Research Council through grant agreement no. 2018-05973.

595 ## Author contributions

596 SS designed and performed the bioinformatics and analyses, which were supervised by DG,
597 OS, IAK, MG, and MB. HH, XL and HZ performed scRNA-seq. SL performed the scRNA-seq
598 data extraction, which was led by DG and MB. SS, DE, MS and YZ analysed the data. SM and
599 AJ were responsible for clinical studies of drug responses in patients with PsA. HW performed
600 the experimental validation. SS, JL, DG, OS, and MB took the lead in writing the manuscript,
601 and all authors provided critical feedback.

602 ## Declaration of interests

603 MB is the scientific founder of Mavatar, Inc. JL is coscientific founder of Scipher Medicine,
604 Inc. DRG is employed by Mavatar, Inc.

605

Material & Methods

scDrugPrio's computational framework

As indicated in **Fig. S1**, scDrugPrio requires 1) an adjusted scRNA-seq matrix, 2) disease-associated differentially expressed genes (DEGs) for each cell type from either group-based comparison of healthy and sick samples or from inflamed and noninflamed samples of one individual, 3) a protein–protein interaction network (PPIN) and 4) drug-target information. scDrugPrio then utilises this information for cell type-specific drug selection, calculation of drug ranking measures and finally rank aggregation.

For drug selection, scDrugPrio first computes the mean closest network distance (d_c) between cell type-specific DEGs and drug targets in the PPIN for each cell type-drug combination. To calculate z-scores (z_c) for network distance, permutation tests (1,000 iterations) were performed in which both cell type-specific DEGs and drug targets were randomised in a bin-adjusted manner (15) before the mean closest distance was calculated. The minimal bin size for randomisation was set at 100 genes. Drugs that did not have any target in the interactome were removed from the analysis (n = 4 for literature-curated PPIN). Based on network distance, we selected only drugs that targets were significantly close ($z_c < -1.64$ corresponding to one-sided $P < 0.05$) to DEGs and that frequently targeted DEGs directly ($d_c < 1$). These cut-offs were chosen based on our empirical observations (**Fig. 3a-d & S2h,j**) and previous knowledge (44). As the significance of network proximity can depend on the number of DEGs relative to the size of the network, cut-offs allowing only the top significant DEGs to enter analysis were implemented when needed. Cell type-specific drug candidates were selected further by requiring drugs to counteract the fold change of at least one targeted DEG. This criterion intuitively removes drugs that likely will not help to restore transcriptomic homeostasis. For

this purpose, the pharmacological action of the drugs on their targets was determined. Binary drug action (activating/enhancing or inhibiting) on the drug target was recorded for each drug (**File 1-5)**. If the pharmacological effect of the drug on the target had not been specified explicitly in DrugBank (19), a literature search was performed using the drug name and gene symbol of the targeted DEG as search terms in PubMed and Google Scholar. Additional information gathered from the literature can be found in **Files 1-5**. In case the pharmacological effect of the drug on a target, despite a literature search, could not be classified as enhancing/activating or inhibiting, the drug target was assumed to not counteract fold-change.

Drug ranking by intra- and intercellular centralities was motivated by empirical observations (**Fig. 3e & S17**) in our study as well as previous indications of the biological importance of disease modules (6, 45) and central cell types in MCDMs (6). For calculation of intracellular centrality, disease modules for each cell type were defined as the largest connected component (LCC) formed by a cell type's DEGs in the PPIN. For LCC identification, the igraph R package (46) was utilised. To avoid overparameterisation, the eigenvector centrality (47) of DEGs in the LCC was calculated using the CINNA R package (48). For each drug, the intracellular centrality was calculated as the geometric mean of its differentially expressed target centrality scores in the cell type-specific LCCs. If a drug did not target any DEG included in the LCC, intracellular centrality was set to zero.

Intercellular centrality was calculated using MCDMs that modelled disease-associated cellular crosstalk. For the creation of MCDMs, first, cell type interactions were predicted using NicheNet (17). Briefly, NicheNet predicts and ranks ligand–target links between interacting cells by combining their expression data with prior knowledge on signalling and gene

regulatory networks. As suggested by Browaeys et al (17), Pearson correlation was used to measure each ligand's ability to predict the gene expression of genes in the *gene set of interest* compared to *background genes* in the receiving cell type. This means that a ligand has a strong positive correlation coefficient if its cognate receptor and the downstream genes of that receptor are all differentially expressed in the downstream cell type. We downloaded the human ligand-target model as well as the human ligand–receptor network (downloaded from https://zenodo.org/record/3260758 April 2020). Cell type-specific DEGs constituted the *gene set of interest*. A set of *potentially active ligands* was defined as the intersection of ligands included in the downloaded human ligand-target model and ligands among respective cell type DEGs. *Background genes* for each cell type were defined as genes (***i***) in the denoised single-cell expression matrix ***D*** of ***k*** cell type-associated cells that showed a mean aggregate expression, ***Ea(i)***, over ***Ea(i)*** $\geq$ 0.2. This definition of background genes was similar to definitions by Browaeys et al. (17) and Puram et al. (49). At the chosen cut-off, we identified ca. 10,000 background genes that corresponded to the recommended amount for NicheNet calculations (17).

$$Ea(i) = \log_2\left(\sum_{j=1}^{k} 10^{D_{ij}}/k\right)$$

All genes were translated to human Entrez gene symbols using human-mouse orthologues downloaded from NCBI (August 2019). Ligand activity analysis in NicheNet was performed for all possible cell type pairs, including self-interactions, excluding cell types that did not express DEGs. In the next step of MCDM construction, directed cell type interactions were derived from ligand activity results and weighted by NicheNet-derived Pearson coefficients.

Only ligand interactions with a positive Pearson correlation coefficient were considered negative Pearson coefficients that reflected the association of a ligand with background genes and therefore were not biologically relevant. The resulting MCDM was visualised using Cytoscape 3.6.1 (50), and for visualisation purposes, the sum of Pearson coefficients that described the directed interaction between two cell types was used. Supplemental analysis supported the relevance of identified ligand interactions (**Supplementary Results**). Eigenvector centrality was calculated for each cell type based on the weighted, directed interactions in the MCDM using the igraph and CINNA R package (46, 48). The intercellular centrality of each drug was computed as the sum of MCDM centralities of the cell types that had selected the drug as a candidate. While eigenvector centrality is well tailored to capture central disease-associated cell types in the MCDM, considering both direct and indirect node connections (47), multiple centrality measures are available. We evaluated several of them, finding them to yield similar results to eigenvector centrality (**Supplementary Results, File 1-5**).

Final rank aggregation involved the calculation of a drug's compounded intra- and intercellular centrality. For this, we calculated combined intracellular centrality for each drug as the sum of drug-specific intracellular centralities in all cell types. The centrality compound score consisted of a drug *intercellular centrality + 0.1 x combined intracellular centrality a*nd thereby emphasised the importance of intercellular centrality over intracellular centrality. Intracellular centrality effectively worked as a tiebreaker. Drugs were ranked based on centrality compound scores, using the average position for ties.

Drug data

We retrieved data on 13,339 drugs from DrugBank (19) (downloaded July 2019) and selected only drugs that had been or currently FDA approved (n = 4,021), were indicated for use in humans (n = 1,964), and had at least one human protein target (n = 1,864). Of those, drug targets could be translated to human Entrez IDs for 1,844 drugs. The drug-target interactions used are provided in **File 1**. Sets of drugs that are approved for each disease were identified according to DrugBank's (19) "Indication" category (**Supplementary Results**, **File 1-3 & 5**). Unless otherwise specified, precision is calculated using these disease-specific sets of FDA-approved drugs as *relevant drugs* or true positives.

For validation of ranked drug candidates, we also downloaded data from www.clinicaltrials.gov (September 2023). Data included information on 465,269 clinical trials registered from September 17th, 1999, to September 7th, 2023. Clinical trials (n = 70,396) for 1,085 of the included 1,844 drugs were found. To derive information on the disease relevance of drug candidates, we filtered clinical trials further by MESH terms, resulting in sets of 724, 494, 532 and 140 drugs that had been tried for rheumatoid arthritis, multiple sclerosis, Crohn's disease and psoriatic arthritis, respectively (**File 1-5**). Even though the outcome of such trials is largely unknown, using drugs registered for clinical trials alongside approved drugs for calculation of precision tests scDrugPrio's ability to capture the pharmacological consensus of the medical community on drugs with an expected effect.

For further validation of drug ranking, we also performed a literature search for the top 100 ranked drug candidates of each data set. We systematically searched PubMed and Google Scholar between June 2020 and December 2022 using the specific disease denotation and the

drug name as search terms. No restrictions or filters were applied. The relevance of the identified articles was screened by title and abstract. When no relevant articles were identified, the drug name was replaced by the substance name, and another search was conducted. To be eligible, studies had to 1) include a control group, 2) be a human clinical study or rodent experiment, 3) measure inflammatory activity and 4) be accessible. When several studies were identified that reported contradictory results, the drug was labelled as having a previously reported effect, reasoning that it would be impossible to determine the evidence and accuracy level in every such instance. In **Files 1-4**, a summary on the nature of the identified article and a full reference is provided, listed by drug.

Precision and recall

$$precision = \frac{\left|\{\text{relevant drugs}\} \cap \{drugs\ in\ selection\}\right|}{\left|\{\text{drugs in selection}\}\right|}$$

$$recall = \frac{\left|\{\text{relevant drugs}\} \cap \{drugs\ in\ selection\}\right|}{\left|\{\text{relevant drugs}\}\right|}$$

When referring to precision among the top 100 candidates, we refer to all candidates with rank ≤ 100.

Protein–protein interaction network

The human interactome was derived from do Valle et al.(51). The literature-curated interactome included 351,444 protein–protein interactions (PPIs) connecting 17,706 unique proteins and was annotated using Entrez Gene IDs. The largest connected component included 351,393 PPIs and 17,651 proteins. Only the largest connected component was used for further analysis.

746

747 *Antigen-induced arthritis mouse model*

748 Antigen-induced arthritis (AIA) was triggered in six 8-week-old, anaesthetised female 129/Sve
749 mice by intra-articular injection of methylated bovine serum (mBSA) in the left knee joint after
750 having presensitised mice to mBSA. The left knee joints of four naïve mice were injected with
751 phosphate-buffered saline (PBS, 20 µL) and used as a negative control. One week after intra-
752 articular triggering of AIA, mice were sacrificed, and joints were either used for
753 immunohistochemistry or scRNA-seq. Histochemical preparation was performed as previously
754 described (6), and specimens were examined in a blinded manner for pannus formation, cartilage
755 and subchondral bone destruction, and synovial hypertrophy on an arbitrary scale, 0–3, as
756 described by Magnusson et al. (52). For the scRNA-seq experiment, joint tissue was minced to
757 ~1 mm^3 pieces, which were digested by collagenase IV (1.5 mg/mL) and DNase I (100 µg/mL)
758 at 37°C. Dissociated cells were passed through a 70-µm cell strainer. Single-cell suspensions
759 were resuspended in RPMI-1640 at a density of 1×10^5 cells/mL for cell loading. One mouse
760 in which AIA had been triggered developed only mild arthritis (arthritis score 0.5) and was
761 therefore excluded from further analysis. All experimental procedures were performed
762 according to the guidelines provided by the Swedish Animal Welfare Act and approved by the
763 Ethical Committee for Research on Animals in Stockholm, Sweden (N271-14).

764

765 scRNA sequencing was performed using the Seq-Well technique (53) following a described
766 protocol (6). Briefly, prepared single-cell suspensions were counted and coloaded with barcoded
767 and functionalised oligo-dT beads (Chemgenes, Wilmington, MA, USA, cat. No. MACOSKO-
768 2011-10) on microwell arrays synthesised as described by Gierahn et al. (53). For each sample,
769 20,000 live cells were loaded per array to bind with oligo-dT beads. Beads were collected for

770 capturing mRNA and preparing the library following cell lysis, hybridisation, reverse
771 transcription and transcriptome amplification. Except for one library, which was sequenced
772 alone, libraries from three samples were pooled for sequencing (**Table S2**), resulting in a
773 coverage of 6.6 reads per base. Four libraries were prepared for each sample using the Nextera
774 XT DNA Library Preparation Kit (Illumina, San Diego, CA, USA; cat. No. FC-131-1096)
775 according to the manufacturer's instructions. Each library was sequenced once, except for one
776 library, which was sequenced twice using the NextSeq 500/550 system.
777
778 The single-cell data were processed into digital gene expression matrices following James
779 Nemesh, McCarrol's lab Drop-seq Core Computational Protocol (version 1.0.1,
780 http://mccarrolllab.com) using *bcl2fastq* Conversion and Picard software. To increase the read
781 depth for the cells, each sample was sequenced multiple times (**Table S2**), and the fastq files
782 for each sample were merged before further alignment steps. The indexed reference for
783 alignment of reads was generated from GRCm38 (June 2017, Ensembl) using STAR software
784 (2.5.3). Only primary alignments towards the reference genome were considered during
785 downstream analyses, according to the mapping quality using STAR software.
786
787 *Sampling and sequencing of psoriatic arthritis patients*
788 *Sampling.* Psoriatic arthritis *(*PsA) patients and controls were recruited by the Immune-
789 Mediated Inflammatory Diseases Consortium (IMIDC) (54). PsA patients were recruited from
790 different rheumatology departments from university hospitals belonging to the IMIDC. All PsA
791 patients were diagnosed according to the CASPAR diagnostic criteria for PsA (55) with > 1
792 year of disease evolution and > 18 years old at the time of recruitment. Exclusion criteria for
793 PsA included the presence of any other form of inflammatory arthritis, rheumatoid factor levels

794 greater than twice the normality threshold or confirmed presence of an inflammatory bowel
795 disease. PBMCs were sampled prior to treatment with anti-TNF or anti-IL17 and cryopreserved.
796 Treatment response was classified at week 12 according to the EULAR response (25) (**File 5**).
797 For the anti-TNF study, 6 males and 10 females were included. The corresponding figures for
798 anti-IL-17 treatment were 3 males (2 responders) and 13 females (6 responders).
799 Simultaneously, healthy age- and sex-matched control subjects (**File 5**) were recruited from
800 healthy volunteers recruited through the Vall d'Hebron University Hospital in Barcelona
801 (Spain). All the controls were screened for the presence of any autoimmune disorder, as well
802 as for first-degree family occurrence of autoimmune diseases. None were found to be positive.
803 Four males and four females were included. The study was approved by the Hospital
804 Universitari Vall d'Hebron Clinical Research Ethics Committee. Protocols were reviewed and
805 approved by the local institutional review board of each participating center.
806
807 *Cell thawing.* PBMCs cryopreserved at -80°C were thawed in a 37°C water bath and transferred
808 with a bored tip to a 15 ml Falcon tube containing 14 ml of 37°C prewarmed RPMI medium
809 supplemented with 10% FBS (Thermo Fisher Scientific). Samples were centrifuged at 300x g
810 for 10 min at (room temperature) RT, the supernatant was removed, and pellets were
811 resuspended in 1 ml of 1X PBS (Thermo Fisher Scientific) supplemented with 1% BSA (PN
812 130-091-376, Miltenyi Biotec) and 10 µL of DNase I (PN LS002007, Worthington-Biochem).
813 After incubation at RT for 10 min with periodic shaking, the cells were filtered with a 20 µm
814 strainer (PN 43-10020-70, Cell Strainer) into a new 15 ml falcon on ice, and the filter was
815 washed by adding 9 mL of cold 1× PBS. Samples were concentrated afterwards by
816 centrifugation at 300 × g for 10 min at 4°C and resuspended in 1 × PBS with 0,05% BSA for
817 further assessment of cell numbers and viability with the TC20™ Automated Cell Counter (Bio-

Rad). Samples balanced by responders and nonresponders for each treatment were mixed in pools of 8 patients at a 50:50 ratio and concentrated by centrifugation in an appropriate volume of 1 × PBS-0.05% BSA to obtain a final cell concentration > 4,000 cells/µL, suitable for 10× Genomics scRNA-sequencing. The suspension was filtered again with a 20 µm strainer, and the cell concentration was verified by counting with the TC20™ Automated Cell Counter.

Cell encapsulation and library preparation. Cells were partitioned into Gel BeadInEmulsions (GEMs) by using the Chromium Controller system (10 × Genomics). Each pooled sample was loaded into two channels with a target recovery of 35,000 cells per channel to ensure a minimum final recovery of 2,000 cells per sample condition. After GEM-RT incubation, the resulting cDNAs were purified with SPRI beads. To ensure maximal cDNA recovery, a second Sylane bead purification was performed on the supernatant from the first purification, and both products were eluted together and preamplified for 13 cycles, following the 10 × Genomics protocol. cDNA was quantified on an Agilent Bioanalyzer High Sensitivity chip (Agilent Technologies), and 100 ng was used for library preparation. Gene Expression (GEX) libraries were indexed with 13 cycles of amplification using the Dual Index Plate TT Set A (10 × Genomics; PN-3000431). The size distribution and concentration of full-length GEX libraries were verified on an Agilent Bioanalyzer High Sensitivity chip. Finally, sequencing of GEX libraries was carried out on a NovaSeq 6000 sequencer (Illumina) using the following sequencing conditions: 28 bp (Read 1) + 10 bp (i7 index) + 10 bp (i5 index) + 90 bp (Read 2) to obtain approximately >20,000 paired-end reads per cell.

3' Single-cell RNA sequencing (scRNA-seq). PBMC samples from 32 patients and 8 healthy controls were evenly mixed in pools of 8 donors per library following a multiplexing approach

based on donor genotype, as in Kang et al. (56), for a more cost- and time-efficient strategy. Importantly, libraries were designed to pool samples together from the same treatment (anti-TNF or anti-IL17) but mixing patients with a different response to treatment. With this approach, we aimed to avoid technical artifacts that could mask subtle biological differences between responders and nonresponders. To profile the cellular transcriptome, we processed the sequencing reads with 10X Genomics Inc. software package CellRanger v6.1.1 and mapped them against the human GRCh38 reference genome.

Library demultiplexing. The donor's genotypes (VCF format) were simplified by removing SNPs that were unannotated or located in the sexual Y, pseudoautosomal XY or mitochondrial chromosomes (chr 0, 24, 25 and 26, respectively). As genotypes were assembled using the human GRCh19 reference genome, we converted them to the same genome assembly used to map the sequencing reads, the human GRCh38 reference genome, using the USCS LiftOver (https://genome.ucsc.edu/cgi-bin/hgLiftOver) command line executable. To meet the LiftOver required format (BED format), we used an available wrapper script (liftOver_vcf.py) to support input/output from VCF format (57). The library demultiplexing by donor was performed with cellsnp-lite v1.2.2 in Mode 1a (57), which allows genotyping single-cell GEX libraries by piling-up the expressed alleles based on a list of given SNPs. To do so, we used a list of 7.4 million common SNPs in the human population (MAF > 5%) published by the 10,00 Genome Project consortium and compiled by Huang et al. (57). Importantly, we used the default parameters, setting the MAF > 5% (--minMAF 0.05) and requesting genotyping in addition to counting (--genotype). Then, we performed donor deconvolution with vireo v0.5.6 (58), which assigns the deconvoluted samples to their donor identity using known genotypes while detecting

865 doublets and unassigned cells. Finally, we discarded detected doublets and unassigned cells
866 before moving on to the downstream processing steps.
867
868 *scRNA-seq data sets and preprocessing*
869 Below, we describe all of the scRNA-seq data sets and the preprocessing steps of the current
870 work as outlined in **Fig. S1**. As most preprocessing steps were applied to scRNA-seq expression
871 matrices of all data sets, we will describe them jointly.
872
873 *Quality cut-offs.* Starting from a raw scRNA-seq gene expression matrix, the quality of cells
874 was assured by application of quality cut-offs that aimed to filter out low-quality cells (few
875 genes, low read depth), dying cells (high expression of mitochondrial genes) and doublets
876 (unexpectedly high reads and large number of genes). While arbitrary, these specific cut-offs
877 were adapted to the corresponding data set and reported in **File 1-5** (59). Genes that were
878 expressed in less than three cells were excluded from further analysis.
879
880 *Batch correction.* In case a high degree of interindividual expression differences existed, batch
881 correction was performed according to a previously established pipeline (60). In short, we used
882 Seurat's function *findIntegrationAnchors()* (61) for the list of objects that corresponded to each
883 individual. These anchors were later used by *IntegrateData()* (61) to integrate the data from
884 individuals to correct for patient-specific differences as suggested in (62).
885
886 *Denoising.* Next, data for all cells were processed by a deep count autoencoder (DCA) model
887 (18), which is a neural network performing a nonlinear principal component analysis (PCA).
888 The DCA method is initiated by computing a library size, log- and z-score normalised

889 expression matrix, which is taken as an input to the neural network, and the output of the neural
890 network log10 transformed), and denoised single-cell expression matrix ***D***, which has the same
891 features as the original data but is corrected for various sources of noise in the data. The DCA
892 method also outputs a representation of the original single-cell data in a latent space. This
893 representation has many fewer features than the original data, which is particularly important
894 for performing accurate cluster analyses. The intercellular expression differences are generally
895 better represented in this latent space than in purely linear PCA models, and the latent space
896 representation is also corrected for single-cell data artefacts such as dropouts and varying
897 library sizes.
898
899 *Clustering analysis* was performed using the Seurat v3.1 package (61) on the DCA-derived
900 latent representation. A shared nearest neighbor graph was constructed, and neighborhood
901 overlap between every cell and its *k*-nearest neighbors was calculated based on the Jaccard
902 index using the *FindNeighbors()* function on all supplied latent features. Next, clusters were
903 identified through application of the Louvain algorithm to the shared nearest neighbor graph
904 using the *FindClusters()* function along with a specified resolution setting. The resolution
905 parameter and *k* for *k*-nearest neighbor analysis were tailored to each data set and are reported
906 below. Clusters were visualised through *RunTSNE ()*.
907
908 *Analyses of interindividual molecular heterogeneity.* After denoising and clustering,
909 heterogeneity among samples was determined. For this, we trained a flexible machine learning
910 model that attempts to find a decision boundary between the given groups of cells. If this model
911 results in a high misclassification rate for test data, it indicates that groups are highly mixed.
912 More specifically, the data were randomly divided in half and used for training and testing the

913 model. A random forest classifier (63) was used to classify cells from sick samples based on
914 what patient the sample was derived from. Cross-validation with 10-fold and grid search (64)
915 was used to find the most appropriate hyperparameters of the random forest. The bootstrap
916 (65)percentile method (65) was used to construct the 95% confidence intervals for training and
917 test misclassification rates. The Scikit package (66) from Python (3.7.9) was used to perform
918 the analysis.
919
920 Furthermore, patient heterogeneity was explored through comparison of cell type proportions
921 and examination of latent features of the non-batch-corrected data. Interindividual differences
922 in cell type proportions were explored by the application of the chi-square test to the proportions
923 of cell types in sick samples. Latent feature comparison was conducted visually through tSNE
924 visualisation of the latent features of each patient. The results for these analyses are found in
925 the **Supplementary Results**.
926
927 *Cell typing.* While cell typing is not crucial for scDrugPrio (which might be performed on
928 unlabelled clusters), we cell typed clusters to enhance biological interpretation. Cell types were
929 assigned to each cluster based on the relative coexpression of several known cell type marker
930 genes. For AIA data, each gene's expression was expressed as a fraction of a cell's total gene
931 expression score. For visualisation of gene expression differences between clusters, z-scores
932 were calculated. Z-scores for single cells were derived by comparison of one cell's gene fraction
933 to all other cells' gene fractions. Z-scores for gene expression of clusters were derived by
934 comparison of the average gene fraction in a cluster to the cluster-averaged gene fractions of
935 cells in other clusters. Murine cell type-specific marker genes for the RA data were derived
936 from the online resources of the R&D systems (www.rndsystems.com/research-area; accessed

July 2020). Cell typing of the human data sets was performed using DCA denoised gene fractions and utilised combinations of marker genes (**File 2 & 3**).

Differentially expressed genes. For each cell type separately, differentially expressed genes (DEGs) were calculated by comparing denoised gene expression of cells derived from healthy samples vs. cells from sick samples. For this purpose, the *FindMarkers()* function in Seurat (61) was used to deploy a scRNA-seq-tailored hurdle model supplied by the MAST package (67). Genes were considered significantly differentially expressed when they showed an absolute log fold change greater than or equal to 1.5 and a Bonferroni-adjusted $P < 0.05$. The fold change cut-off was motivated by previous studies (68) and aimed to decrease the number of DEGs for later network calculations.

Antigen-induced arthritis. Quality cut-offs resulted in a total of 16,751 cells (**File 1**). Genes were annotated as murine NCBI Gene Symbols. Following denoising, clustering using k = 20 and a resolution of 0.6 resulted in the identification of 20 clusters that were cell typed. Heterogeneity analysis used n_estimators = 1,500, max_depth = 15, min_samples_split = 50, and min_samples_leaf = 50 and showed no significant heterogeneity. DEGs and the denoised expression matrix were translated to human Entrez gene IDs using human-mouse orthologues downloaded from NCBI (August 2019).

Multiple sclerosis. A unique molecular identifier (UMI) matrix (22) for cerebrospinal fluid (CSF) of five human multiple sclerosis (MS) patients and five human patients with idiopathic intracerebral hypertension (IIH) were downloaded from the Gene Expression Omnibus (GEO) database (GSE138266). Gene annotation was translated from human Ensembl gene IDs to

961 human Entrez gene IDs and symbols using the HUGO Gene Nomenclature Committee (HGNC)
962 database (69) (downloaded November 2020). After the application of quality cut-offs (**File 2**),
963 we derived 33,848 cells. Initial preprocessing was performed without batch correction using
964 cluster parameters k = 10 and resolution = 0.2 after DCA denoising to derive 17 clusters.
965 Interindividual heterogeneity was assessed as described below using the following
966 hyperparameters: n_estimators = 500, max_depth = 30, min_samples_split = 50,
967 min_samples_leaf = 25. Since we noticed substantial patient-related heterogeneity (**Fig. S5a**),
968 preprocessing was repeated, including batch correction, DCA denoising, and clustering using k
969 = 15 and resolution = 0.35 to derive 21 clusters that were cell typed using known marker genes
970 derived from the original publication (22) (**File 2**). The number of DEGs ranged from 0 to
971 10,076.
972
973 *Crohn's disease.* A unique molecular identifier (UMI) matrix (24) for eleven human Crohn's
974 disease (CD) patients was downloaded from GEO (GSE134809). Data for each patient included
975 intestinal biopsies from one inflamed site and one uninflamed site. After application of quality
976 cut-offs (**File 3**), we derived 77,416 cells. Gene annotation was translated from human Ensembl
977 gene IDs to human Entrez gene IDs and symbols using the HGNC database (2020-11-08) (69).
978 Initially, data were DCA denoised without applying batch correction. Clustering was performed
979 using k = 15 and resolution = 0.8. Interindividual molecular heterogeneity was assessed as
980 described below using the following hyperparameters: n_estimators = 1,000, max_depth = 20,
981 min_samples_split = 50, min_samples_leaf = 25. Since there was substantial interindividual
982 heterogeneity (**Fig. S8a**), preprocessing was repeated now batch-correcting before DCA
983 denoising. Clustering was again performed using k = 15 and resolution = 0.8.
984

Individual Crohn's patients. For individual patient predictions, we used the same quality cut-offs as for the pooled analysis of CD patients. As interindividual heterogeneity does not affect the predictions made for individual patients, these calculations were performed on non-batch-corrected data. DCA denoising was applied to the joint data, and gene annotation was translated to Entrez gene IDs. Thereafter, scRNA-seq data were separated by patient, and cells from each patient were clustered individually. An individual patient cluster was assigned a cell type based on which cluster it most resembled in the joined CD analysis, as measured by the number of shared cell identifiers. DEGs were then calculated between cells from sick and healthy samples. Visualisations of data were in part created using BioRender.com.

Psoriatic arthritis. Data sets were divided into one anti-TNF and one anti-IL17 data set, including responders (R), nonresponders (NR) and healthy controls. We filtered out the doublet and unassigned cells as well as those that did not meet the quality cut-off criteria (**File 5**) and derived 78,610 cells with 5,088 mean reads for the anti-TNF data set and 72,472 cells with 5,343 mean reads for the anti-IL17 data set. In both data sets, 19,415 cells were derived from healthy controls. Data sets were batch-corrected, and DCA was performed. For anti-TNF, clustering was performed using $k = 25$ and resolution = 0.25. The corresponding parameters for anti-IL17 were $k = 15$ and resolution = 0.45. The remaining downstream analysis was performed for responders and nonresponders separately, which meant that DEGs were calculated between responders and healthy controls and between nonresponders and healthy controls. For the anti-TNF data set, the number of DEGs ranged from 0 to 5,989 for R and from 0 to 5,877 for NR. The corresponding figures for anti-IL17 were 0 to 3,097 and 0 to 3,284. Next, scDrugPrio was applied to DEGS from anti-TNF R and NR as well as anti-IL17 R and NR separately.

In vitro validation of potential novel drugs

To validate the predicted novel drugs, *in vitro* culture of murine and human B cells upon activation with the indicated stimuli was employed to assess the effects of the predicted drugs on B-cell survival, activation, proliferation, and antibody production. Three doses for each predicted drug were used to challenge *in vitro* cultured B cells (**Table S1**). For the assessment of potential novel drugs on murine B-cell survival and activation, 300,000 murine naïve B cells ($Lin^-B220^+CD43^-$) were enriched by flow cytometric sorting and cultured in the presence of AffiniPure $F(ab')_2$ Fragment goat anti-mouse anti-IgM (10 µg/mL, CAT: 115-006-075, Jackson ImmunoResearch), anti-mouse CD40 (10 µg/mL, Clone:1C10, Biolegend), or LPS (10 µg/mL) for 24 hours. B-cell survival was determined by flow cytometric analysis of propidium iodide $(PI)^+$ cells. Surface CD69, CD86, and MHC-II were used as readouts for assaying B-cell activation. For the analysis of B-cell proliferation, purified B cells were stained with carboxyfluorescein succinimidyl ester (CFSE) (1 µM) before *in vitro* culture for three days. To determine the effects of the predicted drugs on antibody production, 200,000 purified murine naïve B cells were stimulated with anti-CD40 (10 µg/mL) + IL-4 (10 ng/mL), LPS (10 µg/mL) + IL-4 (10 ng/mL), or LPS (10 µg/mL) + IFN-γ (10 ng/mL) for six days.

For the analysis of novel drugs predicted to regulate the biology of human B cells, peripheral blood mononuclear cells (PBMCs) were isolated from the buffy coat as previously described (70, 71). Human naïve B cells were subsequently preenriched by MACS sorting using a B-Cell Isolation Kit II (Miltenyi) and further purified by flow cytometric sorting of $CD19^+CD27^-$ B cells. Purified human naïve B cells were cultured in 96-well plates in the presence of AffiniPure $F(ab')_2$ Fragment goat anti-human IgG + IgM (5 µg/mL, CAT: 109-006-127, Jackson

ImmunoResearch), anti-human CD40 (5 μg/mL, Clone: G28.5, Bio X Cell), and IL-21 (10 ng/mL, PeproTech).

B-cell survival was determined by flow cytometric analysis of propidium iodide (PI)+- cells. Surface CD69, CD86, and MHC-II were used as readouts for assaying murine B-cell activation. Surface CD69 was assayed for the measurement of human B-cell activation. For the analysis of B-cell proliferation, purified B cells were prestained with carboxyfluorescein succinimidyl ester (CFSE) (1 μM) before *in vitro* culture for three days. Murine IgG2a and IgG1, as well as human IgG in the supernatant, were determined by enzyme-linked immunosorbent assay (ELISA) using goat anti-mouse Ig, goat-anti-mouse IgG1-HRP and goat-anti-human IgG2a-HRP, goat anti-human Ig, and goat-anti-human IgG-HRP (SouthernBiotech) as previously described (72).

In vivo validation of predicted drugs

Amrinone was tested for treating collagen-induced arthritis (CIA). For this, male DBA1/J mice purchased from GemPharmatech (China) were immunised intradermally with 100 μg of chicken type II collagen (2 mg/mL, Chondrex, USA) emulsified with complete Freund's adjuvant (CFA, 1 mg/mL) and boosted on day 21 with 100 μg of chicken type II collagen emulsified with incomplete Freund's adjuvant (IFA). Mice were i.g. given with diluent (n = 5) or amrinone (30 mg/kg, n = 5) daily from day 21 for 3 weeks. The rear paw thickness and the clinical arthritis score for each limb were recorded every other day from 0 to 4 with a maximal score of 16 for each mouse according to the previous protocol (73). Mice were maintained in a specific pathogen-free animal facility at Xuzhou Medical University, and all animal studies

were performed in accordance with protocols approved by the Animal Experimental Ethics Committee of Xuzhou Medical University (202012A162).

Mice were sacrificed on day 21 post drug intervention. Serum was collected for the analysis of collagen-specific autoantibodies by enzyme-linked immunosorbent assay (ELISA) as previously described (74). Briefly, diluted serum was incubated in a 96-well ELISA plate precoated with chicken type II collagen (5 μg/mL). Goat-anti-mouse IgG1-HRP, goat-anti-mouse IgG2a-HRP, and goat-anti-mouse IgG-HRP (SouthernBiotech) were used as detection antibodies. Knee joints were fixed in 4% formaldehyde and subsequently decalcified with decalcification solution (ServiceBio, China) for one week. The specimens were next embedded in paraffin, and sagittal sections (4 μm) were cut. The sections were stained with hematoxylin and eosin (H&E) for the histological analysis of immune cell infiltration and Safranin-O for the analysis of bone erosion as previously described (72, 74).

Comparison of scRNA-seq-based screening outcomes for rheumatoid arthritis to other data types and prediction methods

Briefly, we benchmarked outcomes based on the scRNA-seq-derived DEGs against microarray data (GSE55235 & GSE93272) (75, 76), GWAS Catalog (77) genes and OMIM (78) genes as well as combinations of these data sets. scDrugPrio was compared to previous methods such as 1) identifying druggable DEGs, targeting key enriched pathways (79), CMAP (33) drug predictions and the empirical drug selection of Kim et al. (14). Predictions were also replicated using the smaller, unbiased HuRI PPIN (80) (8,236 proteins, 52,150 interactions) to ensure the absence of knowledge bias. More information can be found in the **Supplementary Results**.

Data and code availability

scRNA-seq data that support the findings of this study are openly available at Gene Expression Omnibus (GEO), reference number GSE193536. Unless otherwise stated, analysis was performed in R 3.6.3. The code for data cleaning and analysis associated with the current submission is available at https://github.com/SDTC-CPMed/scDrugPrio.

References

1. Björnsson B, Borrebaeck C, Elander N, Gasslander T, Gawel DR, Gustafsson M, et al. Digital twins to personalize medicine. Genome Medicine. 2019;12(1):4.
2. Kayal M, Ungaro RC, Bader G, Colombel J-F, Sandborn WJ, Stalgis C. Net Remission Rates with Biologic Treatment in Crohn's Disease: A Reappraisal of the Clinical Trial Data. Clinical Gastroenterology and Hepatology. 2022.
3. Alric H, Amiot A, Kirchgesner J, Tréton X, Allez M, Bouhnik Y, et al. The effectiveness of either ustekinumab or vedolizumab in 239 patients with Crohn's disease refractory to anti-tumour necrosis factor. Alimentary Pharmacology & Therapeutics. 2020;51(10):948-57.
4. Shalek AK, Benson M. Single-cell analyses to tailor treatments. Sci Transl Med. 2017;9(408).
5. Breynaert C, Dresselaers T, Perrier C, Arijs I, Cremer J, Van Lommel L, et al. Unique gene expression and MR T2 relaxometry patterns define chronic murine dextran sodium sulphate colitis as a model for connective tissue changes in human Crohn's disease. PLoS One. 2013;8(7):e68876.
6. Gawel DR, Serra-Musach J, Lilja S, Aagesen J, Arenas A, Asking B, et al. A validated single-cell-based strategy to identify diagnostic and therapeutic targets in complex diseases. Genome Med. 2019;11(1):47.
7. Kim D, Kobayashi T, Voisin B, Jo JH, Sakamoto K, Jin SP, et al. Targeted therapy guided by single-cell transcriptomic analysis in drug-induced hypersensitivity syndrome: a case report. Nat Med. 2020;26(2):236-43.
8. Hsieh C-Y, Wen J-H, Lin S-M, Tseng T-Y, Huang J-H, Huang H-C, et al. scDrug: From single-cell RNA-seq to drug response prediction. Computational and Structural Biotechnology Journal. 2023;21:150-7.
9. Suphavilai C, Chia S, Sharma A, Tu L, Da Silva RP, Mongia A, et al. Predicting heterogeneity in clone-specific therapeutic vulnerabilities using single-cell transcriptomic signatures. Genome Medicine. 2021;13(1):189.
10. Iorio F, Knijnenburg TA, Vis DJ, Bignell GR, Menden MP, Schubert M, et al. A Landscape of Pharmacogenomic Interactions in Cancer. Cell. 2016;166(3):740-54.
11. Corsello SM, Nagari RT, Spangler RD, Rossen J, Kocak M, Bryan JG, et al. Discovering the anticancer potential of non-oncology drugs by systematic viability profiling. Nature Cancer. 2020;1(2):235-48.
12. Freshour SL, Kiwala S, Cotto KC, Coffman AC, McMichael JF, Song JJ, et al. Integration of the Drug-Gene Interaction Database (DGIdb 4.0) with open crowdsource efforts. Nucleic Acids Res. 2021;49(D1):D1144-d51.
13. Li X, Lee EJ, Lilja S, Loscalzo J, Schäfer S, Smelik M, et al. A dynamic single cell-based framework for digital twins to prioritize disease genes and drug targets. Genome Med. 2022;14(1):48.
14. Kim D, Kobayashi T, Voisin B, Jo J-H, Sakamoto K, Jin S-P, et al. Targeted therapy guided by single-cell transcriptomic analysis in drug-induced hypersensitivity syndrome: a case report. Nature Medicine. 2020;26(2):236-43.
15. Guney E, Menche J, Vidal M, Barabasi AL. Network-based in silico drug efficacy screening. Nat Commun. 2016;7:10331.
16. Hughes TR, Marton MJ, Jones AR, Roberts CJ, Stoughton R, Armour CD, et al. Functional discovery via a compendium of expression profiles. Cell. 2000;102(1):109-26.
17. Browaeys R, Saelens W, Saeys Y. NicheNet: modeling intercellular communication by linking ligands to target genes. Nature Methods. 2020;17(2):159-62.
18. Eraslan G, Simon LM, Mircea M, Mueller NS, Theis FJ. Single-cell RNA-seq denoising using a deep count autoencoder. Nature Communications. 2019;10(1):390.

19. Wishart DS, Knox C, Guo AC, Shrivastava S, Hassanali M, Stothard P, et al. DrugBank: a comprehensive resource for in silico drug discovery and exploration. Nucleic Acids Res. 2006;34(Database issue):D668-72.
20. Taylor PC, Feldmann M. Anti-TNF biologic agents: still the therapy of choice for rheumatoid arthritis. Nature Reviews Rheumatology. 2009;5(10):578-82.
21. Rizzi M, Lorenzetti R, Fischer K, Staniek J, Janowska I, Troilo A, et al. Impact of tofacitinib treatment on human B-cells in vitro and in vivo. J Autoimmun. 2017;77:55-66.
22. Schafflick D, Xu CA, Hartlehnert M, Cole M, Schulte-Mecklenbeck A, Lautwein T, et al. Integrated single cell analysis of blood and cerebrospinal fluid leukocytes in multiple sclerosis. Nat Commun. 2020;11(1):247.
23. Hausser-Kinzel S, Weber MS. The Role of B Cells and Antibodies in Multiple Sclerosis, Neuromyelitis Optica, and Related Disorders. Front Immunol. 2019;10:8.
24. Martin JC, Chang C, Boschetti G, Ungaro R, Giri M, Grout JA, et al. Single-Cell Analysis of Crohn's Disease Lesions Identifies a Pathogenic Cellular Module Associated with Resistance to Anti-TNF Therapy. Cell. 2019;178(6):1493-508.e20.
25. Ritchlin CT, Kavanaugh A, Gladman DD, Mease PJ, Helliwell P, Boehncke WH, et al. Treatment recommendations for psoriatic arthritis. Ann Rheum Dis. 2009;68(9):1387-94.
26. Belasco J, Louie JS, Gulati N, Wei N, Nograles K, Fuentes-Duculan J, et al. Comparative genomic profiling of synovium versus skin lesions in psoriatic arthritis. Arthritis Rheumatol. 2015;67(4):934-44.
27. Nerviani A, Boutet MA, Tan WSG, Goldmann K, Purkayastha N, Lajtos TA, et al. IL-23 skin and joint profiling in psoriatic arthritis: novel perspectives in understanding clinical responses to IL-23 inhibitors. Ann Rheum Dis. 2021;80(5):591-7.
28. Lee EJ, Lilja S, Li X, Schäfer S, Zhang H, Benson M. Bulk and single cell transcriptomic data indicate that a dichotomy between inflammatory pathways in peripheral blood and arthritic joints complicates biomarker discovery. Cytokine. 2020;127:154960.
29. FDA U. Paving the way for personalized medicine. FDA's Role in a new Era of Medical Product Development US Department of Health and Human Services. 2013:1-61.
30. Cheng F, Desai RJ, Handy DE, Wang R, Schneeweiss S, Barabási A-Ls, et al. Network-based approach to prediction and population-based validation of in silico drug repurposing. Nature communications. 2018;9(1):1-12.
31. Cheng F, Zhao J, Wang Y, Lu W, Liu Z, Zhou Y, et al. Comprehensive characterization of protein–protein interactions perturbed by disease mutations. Nature Genetics. 2021;53(3):342-53.
32. Kanemaru K, Cranley J, Muraro D, Miranda AMA, Ho SY, Wilbrey-Clark A, et al. Spatially resolved multiomics of human cardiac niches. Nature. 2023;619(7971):801-10.
33. Lamb J, Crawford ED, Peck D, Modell JW, Blat IC, Wrobel MJ, et al. The Connectivity Map: using gene-expression signatures to connect small molecules, genes, and disease. Science. 2006;313(5795):1929-35.
34. Menche J, Guney E, Sharma A, Branigan PJ, Loza MJ, Baribaud F, et al. Integrating personalized gene expression profiles into predictive disease-associated gene pools. npj Systems Biology and Applications. 2017;3(1):10.
35. Nelson SML, Nguyen TM, McDonald JWD, MacDonald JK. Natalizumab for induction of remission in Crohn's disease. Cochrane Database of Systematic Reviews. 2018(8).
36. Needleman SB, Wunsch CD. A general method applicable to the search for similarities in the amino acid sequence of two proteins. Journal of molecular biology. 1970;48(3):443-53.
37. Smith TF, Waterman MS. Identification of common molecular subsequences. Journal of molecular biology. 1981;147(1):195-7.
38. Henikoff S, Henikoff JG. Amino acid substitution matrices from protein blocks. Proc Natl Acad Sci U S A. 1992;89(22):10915-9.

39. Koussounadis A, Langdon SP, Um IH, Harrison DJ, Smith VA. Relationship between differentially expressed mRNA and mRNA-protein correlations in a xenograft model system. Scientific Reports. 2015;5(1):10775.
40. Gillis J, Pavlidis P. The impact of multifunctional genes on" guilt by association" analysis. PloS one. 2011;6(2):e17258.
41. Rusu A, Tanase C, Pascu GA, Todoran N. Recent Advances Regarding the Therapeutic Potential of Adapalene. Pharmaceuticals (Basel). 2020;13(9).
42. Chanani NK, Cowan DB, Takeuchi K, Poutias DN, Garcia LM, del Nido PJ, et al. Differential effects of amrinone and milrinone upon myocardial inflammatory signaling. Circulation. 2002;106(12 Suppl 1):I284-9.
43. Schork NJ. Personalized medicine: Time for one-person trials. Nature. 2015;520(7549):609-11.
44. Cheng F, Kovacs IA, Barabasi AL. Network-based prediction of drug combinations. Nat Commun. 2019;10(1):1197.
45. Özgür A, Vu T, Erkan G, Radev DR. Identifying gene-disease associations using centrality on a literature mined gene-interaction network. Bioinformatics. 2008;24(13):i277-i85.
46. Csardi G, Nepusz T. The igraph software package for complex network research. InterJournal, complex systems. 2006;1695(5):1-9.
47. Negre CFA, Morzan UN, Hendrickson HP, Pal R, Lisi GP, Loria JP, et al. Eigenvector centrality for characterization of protein allosteric pathways. Proc Natl Acad Sci U S A. 2018;115(52):E12201-e8.
48. Ashtiani M, Mirzaie M, Jafari M. CINNA: an R/CRAN package to decipher Central Informative Nodes in Network Analysis. Bioinformatics (Oxford, England). 2018;35.
49. Puram SV, Tirosh I, Parikh AS, Patel AP, Yizhak K, Gillespie S, et al. Single-Cell Transcriptomic Analysis of Primary and Metastatic Tumor Ecosystems in Head and Neck Cancer. Cell. 2017;171(7):1611-24.e24.
50. Shannon P, Markiel A, Ozier O, Baliga NS, Wang JT, Ramage D, et al. Cytoscape: a software environment for integrated models of biomolecular interaction networks. Genome Res. 2003;13(11):2498-504.
51. do Valle IF, Roweth HG, Malloy MW, Moco S, Barron D, Battinelli E, et al. Network medicine framework shows that proximity of polyphenol targets and disease proteins predicts therapeutic effects of polyphenols. Nature Food. 2021;2(3):143-55.
52. Magnusson M, Zare F, Tarkowski A. Requirement of type I interferon signaling for arthritis triggered by double-stranded RNA. Arthritis Rheum. 2006;54(1):148-57.
53. Gierahn TM, Wadsworth MH, 2nd, Hughes TK, Bryson BD, Butler A, Satija R, et al. Seq-Well: portable, low-cost RNA sequencing of single cells at high throughput. Nat Methods. 2017;14(4):395-8.
54. Aterido A, Cañete JD, Tornero J, Ferrándiz C, Pinto JA, Gratacós J, et al. Genetic variation at the glycosaminoglycan metabolism pathway contributes to the risk of psoriatic arthritis but not psoriasis. Ann Rheum Dis. 2019;78(3).
55. Taylor W, Gladman D, Helliwell P, Marchesoni A, Mease P, Mielants H. Classification criteria for psoriatic arthritis: development of new criteria from a large international study. Arthritis Rheum. 2006;54(8):2665-73.
56. Kang HM, Subramaniam M, Targ S, Nguyen M, Maliskova L, McCarthy E, et al. Multiplexed droplet single-cell RNA-sequencing using natural genetic variation. Nature biotechnology. 2018;36(1):89-94.
57. Huang X, Huang Y. Cellsnp-lite: an efficient tool for genotyping single cells. Bioinformatics. 2021;37(23):4569-71.
58. Huang Y, McCarthy DJ, Stegle O. Vireo: Bayesian demultiplexing of pooled single-cell RNA-seq data without genotype reference. Genome Biol. 2019;20(1):273.
59. Luecken MD, Theis FJ. Current best practices in single-cell RNA-seq analysis: a tutorial. Mol Syst Biol. 2019;15(6):e8746.

60. Stuart T, Butler A, Hoffman P, Hafemeister C, Papalexi E, Mauck WM, et al. Comprehensive Integration of Single-Cell Data. Cell. 2019;177(7):1888-902.e21.
61. Butler A, Hoffman P, Smibert P, Papalexi E, Satija R. Integrating single-cell transcriptomic data across different conditions, technologies, and species. Nature Biotechnology. 2018;36(5):411-20.
62. Luecken MD, Büttner M, Chaichoompu K, Danese A, Interlandi M, Mueller MF, et al. Benchmarking atlas-level data integration in single-cell genomics. Nature Methods. 2022;19(1):41-50.
63. Breiman L. Random forests. Machine learning. 2001;45(1):5-32.
64. Krstajic D, Buturovic LJ, Leahy DE, Thomas S. Cross-validation pitfalls when selecting and assessing regression and classification models. Journal of cheminformatics. 2014;6(1):1-15.
65. Efron B, Tibshirani RJ. An introduction to the bootstrap: CRC press; 1994.
66. Pedregosa F, Varoquaux G, Gramfort A, Michel V, Thirion B, Grisel O, et al. Scikit-learn: Machine learning in Python. the Journal of machine Learning research. 2011;12:2825-30.
67. Finak G, McDavid A, Yajima M, Deng J, Gersuk V, Shalek AK, et al. MAST: a flexible statistical framework for assessing transcriptional changes and characterizing heterogeneity in single-cell RNA sequencing data. Genome biology. 2015;16(1):278.
68. Zhao B, Erwin A, Xue B. How many differentially expressed genes: A perspective from the comparison of genotypic and phenotypic distances. Genomics. 2018;110(1):67-73.
69. Tweedie S, Braschi B, Gray K, Jones TEM, Seal RL, Yates B, et al. Genenames.org: the HGNC and VGNC resources in 2021. Nucleic Acids Res. 2021;49(D1):D939-d46.
70. Shi Y, Xu M, Pan S, Gao S, Ren J, Bai R, et al. Induction of the apoptosis, degranulation and IL-13 production of human basophils by butyrate and propionate via suppression of histone deacetylation. Immunology. 2021;164(2):292-304.
71. He C, Gao S, Zhao X, Shi Y, Tang Y, Cao Y, et al. An efficient and cost-effective method for the purification of human basophils. Cytometry A. 2022;101(2):150-8.
72. Li H, Tang Y, Ren J, Bai R, Hu L, Jia W, et al. Identification of novel B-1 transitional progenitors by B-1 lymphocyte fate-mapping transgenic mouse model Bhlhe41 (dTomato-Cre). Front Immunol. 2022;13:946202.
73. Brand DD, Latham KA, Rosloniec EF. Collagen-induced arthritis. Nat Protoc. 2007;2(5):1269-75.
74. Park SH, Rhee J, Kim SK, Kang JA, Kwak JS, Son YO, et al. BATF regulates collagen-induced arthritis by regulating T helper cell differentiation. Arthritis Res Ther. 2018;20(1):161.
75. Woetzel D, Huber R, Kupfer P, Pohlers D, Pfaff M, Driesch D, et al. Identification of rheumatoid arthritis and osteoarthritis patients by transcriptome-based rule set generation. Arthritis Res Ther. 2014;16(2):R84.
76. Tasaki S, Suzuki K, Kassai Y, Takeshita M, Murota A, Kondo Y, et al. Multi-omics monitoring of drug response in rheumatoid arthritis in pursuit of molecular remission. Nature communications. 2018;9(1):2755-.
77. Buniello A, MacArthur JAL, Cerezo M, Harris LW, Hayhurst J, Malangone C, et al. The NHGRI-EBI GWAS Catalog of published genome-wide association studies, targeted arrays and summary statistics 2019. Nucleic Acids Res. 2019;47(D1):D1005-d12.
78. Amberger J, Bocchini CA, Scott AF, Hamosh A. McKusick's Online Mendelian Inheritance in Man (OMIM). Nucleic Acids Res. 2009;37(Database issue):D793-6.
79. Kanehisa M. Toward understanding the origin and evolution of cellular organisms. Protein Sci. 2019;28(11):1947-51.
80. Luck K, Kim D-K, Lambourne L, Spirohn K, Begg BE, Bian W, et al. A reference map of the human binary protein interactome. Nature. 2020;580(7803):402-8.